ACS ORGANIC & INORGANIC Au
AN OPEN ACCESS JOURNAL OF THE AMERICAN CHEMICAL SOCIETY

pubs.acs.org/orginorgau
Article

Controlling Redox and Wirelike Charge-Delocalization Properties of Dinuclear Mixed-Valence Complexes with MCp*(dppe) (M = Fe, Ru) Termini Bridged by Metalloporphyrin Linkers

Published as part of ACS Organic & Inorganic Au virtual special issue "Electrochemical Explorations in Organic and Inorganic Chemistry".

Masahito Murai, Masanori Ono, Yuya Tanaka, and Munetaka Akita*

Cite This: ACS Org. Inorg. Au 2024, 4, 504−516
Read Online

ACCESS | Metrics & More | Article Recommendations | Supporting Information

ABSTRACT: Four dinuclear organometallic molecular wire complexes with diethynylmetalloporphyrin linkers $\mathbf{1}^{MM'}$, [5,15-bis{MCp*(dppe)ethynyl}-10,20-diarylporphinato]M' (Cp* = η^5-C_5Me_5; dppe = 1,2-bis(diphenylphosphino)-ethane; M/M' = Fe/Zn ($\mathbf{1}^{FeZn}$), Ru/Zn ($\mathbf{1}^{RuZn}$), Fe/Ni ($\mathbf{1}^{FeNi}$), Ru/Ni ($\mathbf{1}^{RuNi}$); aryl = 3,5-di-*tert*-butylphenyl), are synthesized and characterized by NMR, CV, UV−vis-NIR, and ESI-TOF mass spectrometry techniques. Electrochemical investigations combined with electronic absorption spectroscopic studies reveal strong interactions among the electron-donating, redox-active MCp*(dppe) termini and the metalloporphyrin moieties. The monocationic species of the four complexes obtained by chemical oxidation have been characterized as mixed-valence Class II/III or Class III compounds according to the Robin-Day classification despite the long molecular dimension (>1.5 nm), as demonstrated by their intense intervalence charge transfer bands (IVCT) in the near IR region. DFT calculations indicate large spin densities on the metalloporphyrin moieties. Furthermore, the wirelike performance can be finely tuned by coordination of appropriate nitrogen donors to the axial sites of the metalloporphyrin.

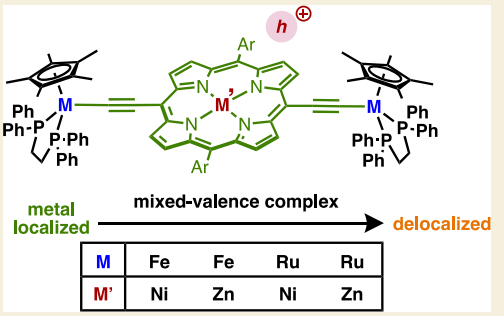

KEYWORDS: *molecular wire, mixed valence species, porphyrin, acetylide, iron, ruthenium*

INTRODUCTION

Mixed-valence (MV) complexes consisting of plural metal atoms with different oxidation states have been studied as carrier transfer systems for molecular electronics, i.e. as molecular wires.[1−3] Common MV complexes consist of two redox-active metal centers connected by a bridging ligand (BL), and their wire-like performance has been evaluated on the basis of the properties of the corresponding MV radical cations or anions, $[ML_n\text{-BL-}ML_n]^{\pm\bullet}$, obtained upon 1e-redox processes (*vide infra*) (Figure 1a).[4−6] Among these, the metal acetylide MV complexes of iron and ruthenium with electron-donating ligands susceptible to 1e-oxidation have been extensively explored for two decades due to their rich redox behavior as well as the resultant stable oxidized monocationic species.[7−11] These MV complexes have been considered to be model structures of molecular junctions, i.e. metal electrode-molecule-metal electrode composites, being a minimum component of molecular electronics. Although the relationship between MV complexes and molecular junctions is complicated, as discussed by Launay,[12] recent interest has shifted toward these metal complexes being directly used as components in molecular junctions.[13−30] Therefore, investigation of charge-delocalized properties of MV complexes themselves remains of fundamental importance for both models and components in molecular electronics.

The charge delocalization properties, i.e. wirelike behavior, can be effectively controlled by appropriate design of the BL, such as substituents,[31−35] π-extension,[36−41] metal complexation,[37,42] and various external stimuli.[43−47] However, the interactions between the two metal centers usually deteriorate exponentially upon extension of the BL.[48] In this context, polyyne-diyl complexes $ML_n\text{-}(C{\equiv}C)_m\text{-}ML_n$ have been expected to show long-range electronic interaction between the terminal metal fragments due to the interactions of the two perpendicularly oriented π-systems of the polyynediyl bridge with the metal d orbitals.[49−56] The corresponding 1e-oxidized MV complexes, however, are thermally unstable due to the high radical reactivity of the carbon chains[57,58] and, thus, their

Received: April 5, 2024
Revised: July 1, 2024
Accepted: July 3, 2024
Published: July 15, 2024

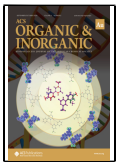

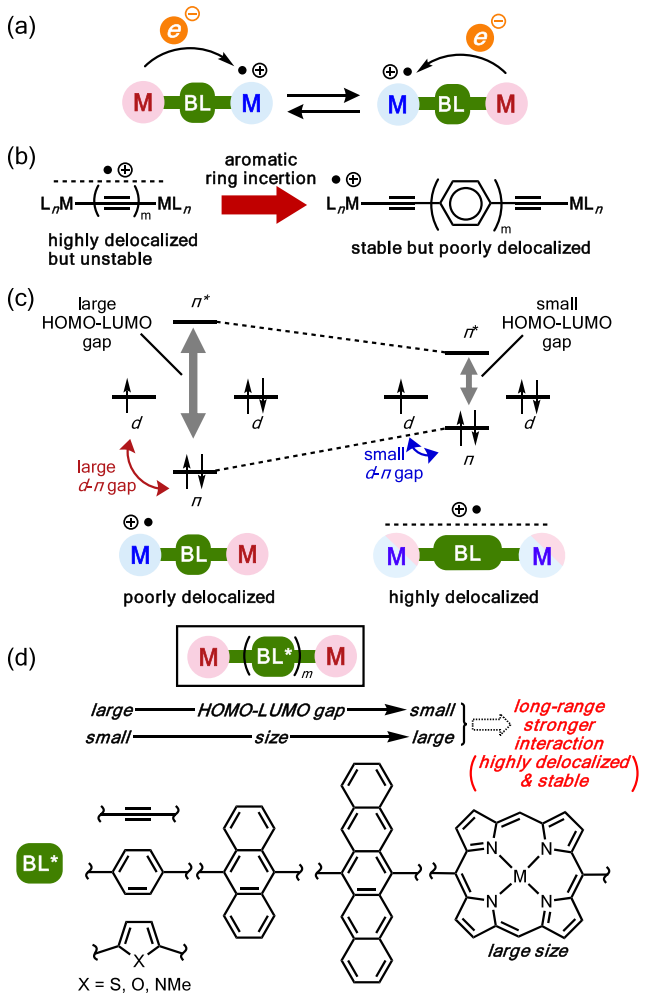

Figure 1. (a) Electron transfer processes of mixed-valence (MV) complexes. (b) Charge-delocalized properties of $[ML_n\text{-}(C{\equiv}C)_m\text{-}ML_n]^{+\bullet}$ and $[ML_n\text{-}C{\equiv}C\text{-}(p\text{-}C_6H_4)_m\text{-}C{\equiv}C\text{-}ML_n]^{+\bullet}$. (c) Orbital diagrams for MV complexes with large and small HOMO−LUMO gaps. (d) Representative bridging ligands employed for the studies of metal acetylide-based MV complexes $[ML_n\text{-}(BL)_m\text{-}ML_n]^{+\bullet}$.

propensity to support long-range electron transfer has remained unclear (Figure 1b).[59] Stability of the MV complexes can be improved by introduction of phenylene rings $ML_n\text{-}C{\equiv}C\text{-}(p\text{-}C_6H_4)_m\text{-}C{\equiv}C\text{-}ML_n$[60,61] but their wirelike performance is not always good because one of the dπ-pπ interactions was interfered by the inserted sp^2 -hybridized phenyl rings. Another reason lies in the aromaticity, which deteriorates the π-conjugation of the BL.[8,62] The large HOMO−LUMO energy gaps of the πconjugated linker also leads to less effective orbital interaction between the electron-rich metal termini and the BL (Figure 1c).[41] Therefore, achieving effective long-range (>1 nm) carrier transport on stable MV systems remains challenging.

For the dinuclear metal acetylide MV complexes, $[ML_n\text{-}C{\equiv}C\text{-}(BL^*)_m\text{-}C{\equiv}C\text{-}ML_n]^{+\bullet}$, various aromatic bridging units (BL*) including phenylene, heteroarylene, anthrylene, and higher acetylenes have been examined (Figure 1d). The degree of charge-delocalization increases with narrowing the HOMO−LUMO gaps of the BLs. These studies, thus, prompted us to examine MV complexes with BLs with narrow HOMO−LUMO gaps. Herein, we report on the design of new MV systems $[\mathbf{1}^{MM'}]^{+\bullet}$ consisting of the two MCp*(dppe) fragments (M = Fe, Ru; Cp* = η^5-C_5Me_5; dppe = 1,2-diphenylphosphinoethane) bridged by the zinc- and nickel-porphyrin-containing linkers (Figure 2a). Porphyrin motifs with the large dimensions are widely utilized in nature and materials chemistry,[63−68] key components for charge and energy carrier transport systems, and their highly π−delocalized systems with the small HOMO−LUMO gaps bring the frontier orbitals closer to the energy levels of the metal fragments to lead to stronger long-range metal-BL interaction, i.e. a nm-order highly delocalized system (>1 nm) (Figure 1d). Furthermore, modulation of the frontier orbital energies could be achieved by the choice of the metal centers embedded in the porphyrins.[69−73] In this study, we have found that the combination of the metal acetylide MV systems and the metalloporphyrins leads to highly delocalized and stable MV systems as well as wide variation of their redox and charge-delocalized behavior. This reflects that the Zn and Ni centers embedded in the porphyrin BL* can also act as efficient modulators for the properties of the dinuclear organometallic wire.[74−77]

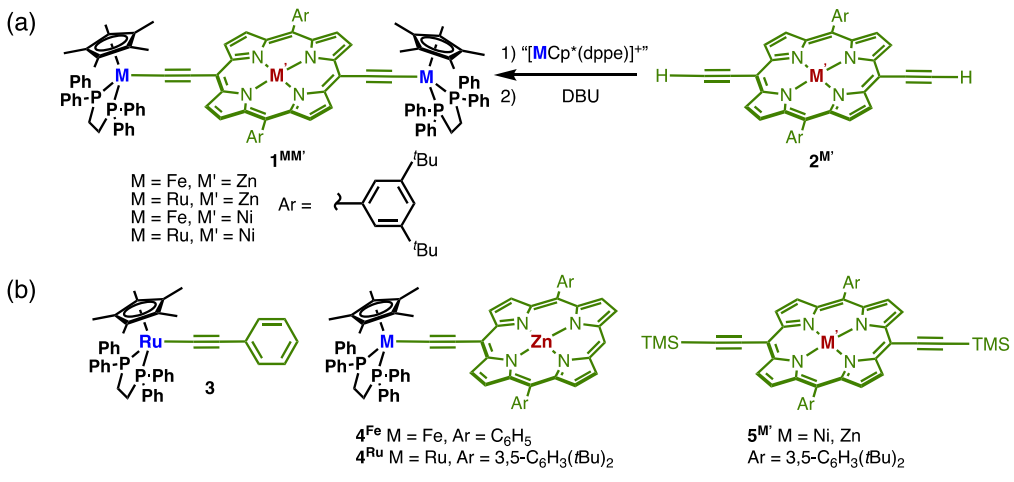

Figure 2. (a) Structures and synthesis of iron- and ruthenium-porphyrin molecular wires $\mathbf{1}^{MM'}$. (b) Structures of reference complexes.

https://doi.org/10.1021/acsorginorgau.4c00021
ACS Org. Inorg. Au 2024, 4, 504−516

RESULT AND DISCUSSION

Synthesis

A series of dinuclear iron- and ruthenium-acetylide complexes with the porphyrin linkers $\mathbf{1}^{MM'}$ (M/M' = Fe/Zn ($\mathbf{1}^{FeZn}$), Ru/Zn ($\mathbf{1}^{RuZn}$), Fe/Ni ($\mathbf{1}^{FeNi}$), Ru/Ni ($\mathbf{1}^{RuNi}$)) was prepared by the reaction of [5,15-di(ethynyl)-10,20-bis(3,5-di(*tert*-butyl)-phenyl)porphinato]zinc(II) $\mathbf{2}^{Zn}$ or its nickel analogue $\mathbf{2}^{Ni}$ with the cationic $[MCp^*(dppe)]^{+\bullet}$ species generated *in situ*, followed by deprotonation of the resultant bis-vinylidene intermediates with DBU (Figure 2a). The symmetrical structures of conjugates $\mathbf{1}^{MM'}$ were well-characterized by ^1H and ^{31}P NMR spectroscopy, elemental analysis, ESI-TOF-MS, and IR spectroscopies. These complexes turned out to be stable at room temperature under nitrogen atmosphere with no apparent decomposition even after 6 months. A solid-state structure of the nickelporphyrinato-ruthenium complex $\mathbf{1}^{RuNi}$ is shown in Figure 3. The porphyrin core shows a large distortion

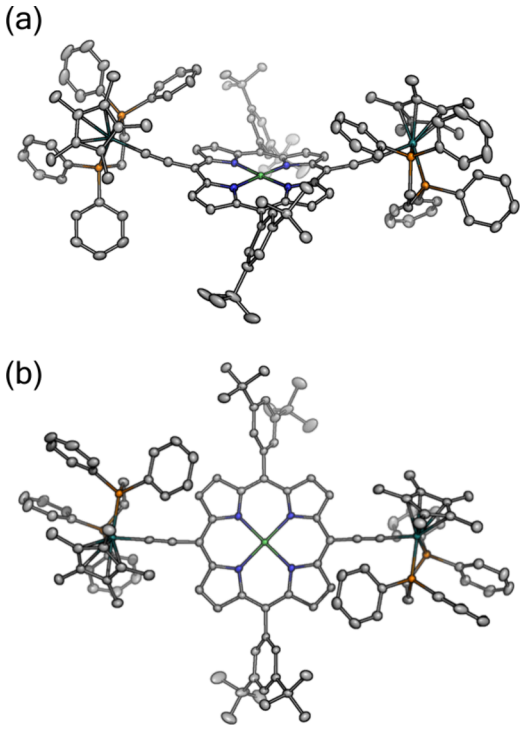

Figure 3. ORTEP drawings of $\mathbf{1}^{RuNi}$, (a) side and (b) top views. Hydrogen atoms and solvents are omitted for clarity. Thermal ellipsoids were set at the 50% probability level.

from the planarity as indicated by the Ru−Ni−Ru angle of 151°, while the Ni atom adopts a square-planar geometry (the sum of ∠N−Ni−N ∼ 360°). Such a distortion of the Ni porphyrin core is frequently observed for those with large substituents at the meso positions.[78] The bond alternations of the metalloporphyrin core are similar to those for the previously reported counterparts.[79] On the other hand, the Ru−C_α (1.988(4) Å) and C_β-C_γ bond lengths (1.419(6) Å) in the Ru−C_α ≡ C_β-C_γ linkage are shorter than those for the phenylethynyl derivative Cp*(dppe)Ru−C≡C-Ph **3** (2.011(4) and 1.431(5) Å, respectively),[80] whereas the C_α ≡ C_β bond distance (1.226(6) Å) is longer than that of **3** (1.215(5) Å). The distortion suggested that the back-donation from the Ru center to the acetylide moieties in $\mathbf{1}^{RuNi}$ is stronger than that in **3**, as is caused by the lower-lying LUMO of the Ni porphyrin core receiving the back-donation (*vide infra*). The through-space distance between the two Ru centers was determined to be 15.5 Å.

Charge Delocalization

The extent of charge delocalization and intermetallic interactions of 1e-oxidized radical cations of dinuclear species, i.e. wirelike performance, can be evaluated on the basis of the spectroscopic parameters (V_{ab}: electronic coupling (IVCT band); *g* tensors (ESR)).

i) Electrochemistry. Electrochemistry of the complexes **1** was examined by cyclic voltammetry and the results were compared with the corresponding monoacetylide complexes $\mathbf{4}^{M}$ (M = Fe, Ru),[81] and the trimethylsilyl derivatives without the metal termini $\mathbf{5}^{M'}$ (M' = Ni, Zn) (Figures 2b, 4 and Table 1). All four porphyrin complexes $\mathbf{1}^{MM'}$ showed two well-separated reversible one-electron redox processes in the range between −200 and −1000 mV (vs. $[FeCp_2]/[FeCp_2]^+$ couple) along with one-electron redox processes in the range from 100 to 500 mV. The former were related to the M^{II}/M^{III} redox processes (M = Fe, Ru), while the latter were assigned to the oxidation waves of the porphyrin moieties because the

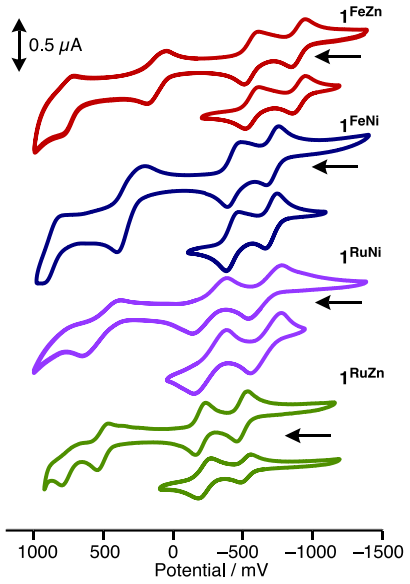

Figure 4. Cyclic voltammograms of $\mathbf{1}^{MM'}$. ([complex] = 1 mM in CH_2Cl_2, $NBu_4^+PF_6^-$ = 0.1 M, working and counter electrode; Pt, reference electrode; $Ag/AgNO_3$, 298 K, plotted as polarographic convention).

Table 1. CV Data for 1−5[a]

	$E_{1/2}^{M1}$	$E_{1/2}^{M2}$	ΔE[b]	K_C[c]	$E_{1/2}^{por}$
$\mathbf{1}^{FeZn}$	−902	−562	340	5.7×10^5	118
$\mathbf{1}^{RuZn}$	−656	−261	395	4.8×10^6	513
$\mathbf{1}^{FeNi}$	−714	−444	270	3.7×10^4	336
$\mathbf{1}^{RuNi}$	−495	−195	300	1.2×10^5	514
$\mathbf{4}^{Fe}$[d]	−591				129
$\mathbf{4}^{Ru}$[d]	−315				105
$\mathbf{5}^{Zn}$					539
$\mathbf{5}^{Ni}$					500

[a][Complex] = 1 mM in CH_2Cl_2, $NBu_4{\cdot}PF_6$ = 0.1 M, W.E., C.E = Pt, R.E. $Ag/AgNO_3$, [b]$\Delta E = E_{1/2}^{M2} - E_{1/2}^{M1}$, [c]$K_C = \exp(F\bullet\Delta E/RT)$, [d]Ref 81.

https://doi.org/10.1021/acsorginorgau.4c00021
ACS Org. Inorg. Au 2024, 4, 504−516

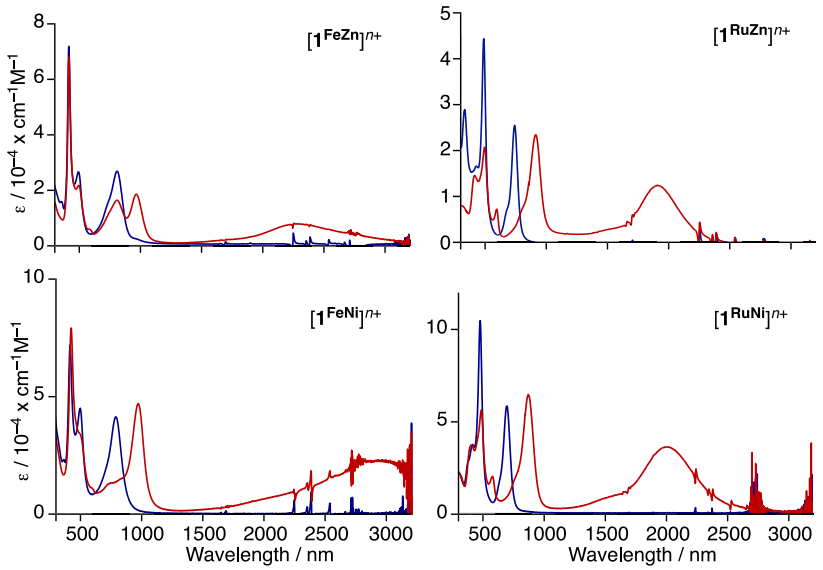

Figure 5. UV−vis-NIR spectra for $[\mathbf{1}^{MM'}]^{n(+\bullet)}$ observed in CH_2Cl_2 (blue: neutral (n = 0); red: monocation (n = 1)).

porphyrin complexes $\mathbf{5}^{M'}$ (M' = Ni, Zn) showed the oxidation waves around 500 mV. The comproportionation constant K_C indicating the thermodynamic stability of 1e-oxidized, mixed-valence species was determined on the basis of the ΔE values ($E_{1/2}{}^{M2}-E_{1/2}{}^{M1}$), as summarized in Table 1. Despite the very long nm-order distances separating the two metal centers (>1.5 nm), these complexes showed the large ΔE and K_C values (K_C > 10^4). The K_C values for Ru complexes $\mathbf{1}^{Ru,M}$ are larger than those for the Fe complexes $\mathbf{1}^{Fe,M}$, and the Ru−Zn complex $\mathbf{1}^{RuZn}$ shows the largest K_C value (4.8×10^6) among them. Interpretation of K_C values should be careful especially for MV complexes with different metal fragments, because half-wave potential separations and the derived K_C values depend on several parameters, including ion-pairing, solvation, electrolytes, magnetic exchange interactions and so on.[82,83] Nevertheless, the large K_C values indicate that the corresponding radical cations are thermodynamically stable with respect to disproportionation.

When compared to the silyl-terminated zinc complex $\mathbf{5}^{Zn}$, the oxidation process of the porphyrin moiety ($E_{1/2}{}^{por}$) of the iron complex $\mathbf{1}^{FeZn}$ was cathodically shifted by 421 mV (118 ($\mathbf{1}^{FeZn}$) vs 539 mV ($\mathbf{5}^{Zn}$)), indicating the significant electron donating ability of the peripheral iron fragments to the metalloporphyrin core through the C≡C units. On the other hand, the corresponding oxidation wave of the ruthenium complex $\mathbf{1}^{RuZn}$ was observed at 513 mV, which is close to that of $\mathbf{5}^{Zn}$. These trends were similarly observed for the Ni-porphyrin analog, where the porphyrin oxidation potential of $\mathbf{1}^{FeNi}$ was cathodically shifted by 164 mV compared to $\mathbf{5}^{Ni}$ ($\mathbf{1}^{FeNi}$; 336 mV, $\mathbf{5}^{Ni}$; 500 mV), while that of $\mathbf{1}^{RuNi}$ (514 mV) was almost identical with each other. These results indicated that the electron-donating power of the FeCp*(dppe) unit is much stronger than that of the RuCp*(dppe) unit as already noted for related systems.

ii) UV−Vis-NIR studies. The monocationic complexes $[\mathbf{1}^{MM'}]^{+\bullet}$ were prepared by stoichiometric chemical oxidation of $\mathbf{1}^{MM'}$ with ferrocenium hexafluorophosphate, $[FeCp_2]PF_6$ (Scheme S1). They turned out to be stable at ambient temperature under a nitrogen atmosphere and were subjected to UV−vis-NIR measurements. The obtained spectra and data for the neutral and oxidized species are shown in Figure 5 and Table 2, respectively. For the neutral species, the strong absorption bands observed around 500 and 700−800 nm are attributed to the Soret and Q-bands of the metalloporphyrin cores, respectively. The prominent red-shifts of the Q-bands for $\mathbf{1}^{FeZn}$ (815 nm) and $\mathbf{1}^{RuZn}$ (733 nm) compared to the corresponding metalloporphyrin counterparts $\mathbf{5}^{Zn}$ (595 nm) suggests that the metal acetylide parts significantly contribute to the frontier orbitals. Chemical 1e-oxidation of the neutral species $\mathbf{1}^{MM'}$ causes red-shifts of the Q-bands by about 200 nm as well as the appearance of the new absorptions at 2271 ($[\mathbf{1}^{FeZn}]^{+\bullet}$), 1891 ($[\mathbf{1}^{RuZn}]^{+\bullet}$), 2952 ($[\mathbf{1}^{FeNi}]^{+\bullet}$), and 1892 nm ($[\mathbf{1}^{RuNi}]^{+\bullet}$) in the near IR region, which are assigned to the IVCT bands. Such absorptions were not observed for the monocationic species of monometal acetylide derivatives ($[\mathbf{4}^{M}]^{+\bullet}$).[81] We carried out deconvolution analysis of the IVCT bands of monocations $[\mathbf{1}^{MM'}]^{+\bullet}$, and the lowest-enegy bands were used for further analysis (Figure 6 and Table 3). The half-height widths ($\nu_{1/2}{}^{exp}$) of the IVCT bands for $[\mathbf{1}^{MM'}]^{+\bullet}$ obtained by deconvolution analysis are much narrower than the calculated half-height widths $\nu_{1/2}{}^{calcd}$, indicating that the monocationic species are Class III species according to the Robin-Day classification.[14] For the quantitative discussion, we have used Γ values proposed by Brunschwig et al.[84]

Table 2. UV−Vis-NIR Data for $[\mathbf{1}^{MM'}]^{n(+\bullet)}$ Observed in CH_2Cl_2

complex	λ_{max}/nm ($\varepsilon \times 10^{-3}$/$M^{-1}cm^{-1}$)
$\mathbf{1}^{FeZn}$	422 (75.2), 501 (27.5), 815 (27.8)
$[\mathbf{1}^{FeZn}]^{+\bullet}$	424 (71.3), 510 (21.7), 820 (16.8), 979 (18.8), 2271 (7.9)
$[\mathbf{1}^{FeZn}]^{2+}$	441 (67.1), 795 (12.5), 1032 (22.9), 1139 (sh, 18.6)
$\mathbf{1}^{RuZn}$	324 (29.2), 481 (44.3), 733 (25.7)
$[\mathbf{1}^{RuZn}]^{+\bullet}$	429 (46.5), 483 (40.1), 707 (15.6), 897 (11.2), 1891 (4.1)
$[\mathbf{1}^{RuZn}]^{2+}$	430 (16.1), 501 (20.0), 1143 (1.99)
$\mathbf{1}^{FeNi}$	419 (71.3), 501 (44.9), 784 (44.1)
$[\mathbf{1}^{FeNi}]^{+\bullet}$	425 (79.4), 971 (4.71), 2952 (23.0)
$[\mathbf{1}^{FeNi}]^{2+}$	442 (97.8), 750 (17.7), 1000 (36.6)
$\mathbf{1}^{RuNi}$	421 (37.8), 481 (106), 729 (22.9)
$[\mathbf{1}^{RuNi}]^{+\bullet}$	408 (3.75), 491 (56.9), 582 (20.2), 875 (64.2), 1892 (12.6)
$[\mathbf{1}^{RuNi}]^{2+}$	430 (76.1), 501 (49.0), 762 (11.7), 1131 (46.8)

https://doi.org/10.1021/acsorginorgau.4c00021
ACS Org. Inorg. Au 2024, 4, 504−516

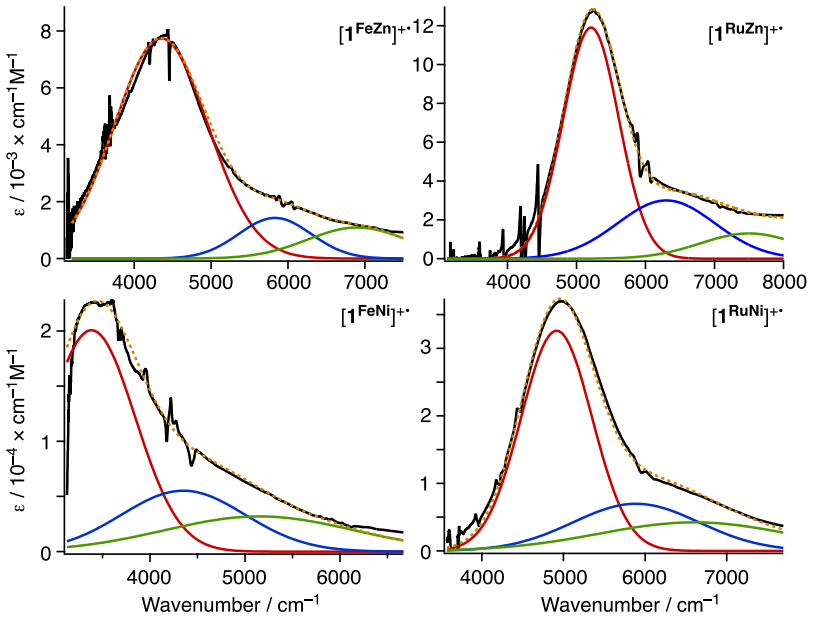

Figure 6. NIR absorption spectra for $[\mathbf{1}^{MM'}]^{+\bullet}$ in CH_2Cl_2 (plane black) and the deconvoluted IVCT bands (dashed curves: the sum of the deconvoluted curves; plain red, blue, and green curves: deconvoluted curves).

Table 3. Parameters Obtained by Deconvolution Analysis for $[\mathbf{1}^{MM'}]^{+\bullet}$

complex	ν_{max} (cm^{-1})	ε ($M^{-1}cm^{-1}$)	$\nu_{1/2}^{exp}$ (cm^{-1})	$\nu_{1/2}^{calc}$ (cm^{-1})[a]	Γ[b]	V_{ab}(Class II) (cm^{-1})[c]	V_{ab}(Class III) (cm^{-1})[d]
$[\mathbf{1}^{FeZn}]^{+\bullet}$	4350	7753	1230	3170	0.61	259	2175
$[\mathbf{1}^{RuZn}]^{+\bullet}$	5210	10800	570	3469	0.84	241	2605
$[\mathbf{1}^{FeNi}]^{+\bullet}$	3383	23000	922	2773	0.67	336	1692
$[\mathbf{1}^{RuNi}]^{+\bullet}$	4915	36500	863	3370	0.74	522	2457

[a]Calculated from the Hush formula for a class II compound ($\nu_{1/2}^{calc} = (2310\ \nu_{max})^{1/2}$). [b]$\Gamma = 1 - \nu_{1/2}^{exp}/\nu_{1/2}^{calc}$. [c]Evaluated as Class II compounds ($V_{ab} = 2.06 \times 10^{-2} \times (\nu_{max} \bullet \varepsilon_{max} \bullet \nu_{1/2})/d_{M\text{-}M}$), where $d_{M\text{-}M}$ was extracted from the DFT optimized structures. [d]Calculated for a Class III compound ($V_{ab} = \nu_{max}/2$).

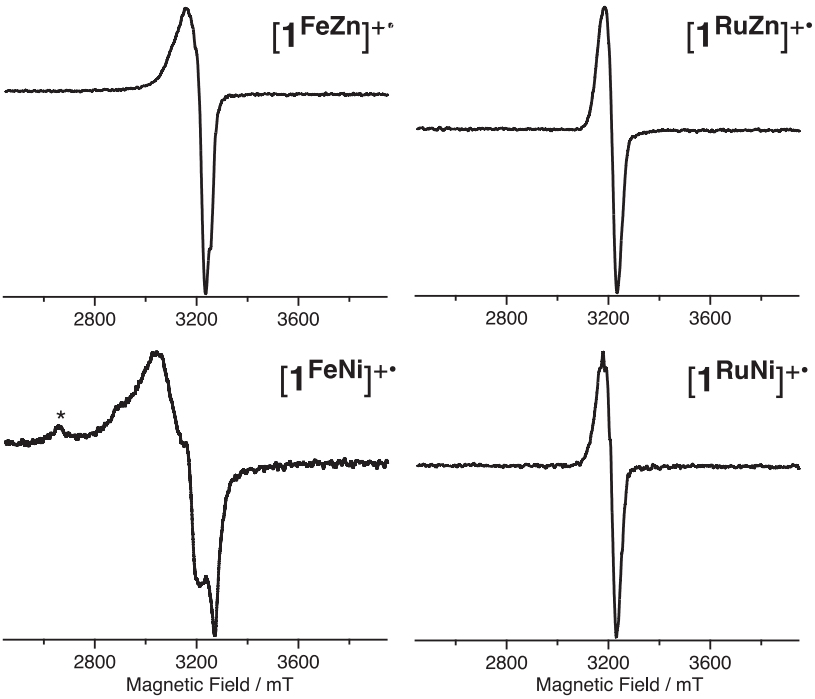

Figure 7. ESR spectra of $[\mathbf{1}^{MM'}]^{+\bullet}$ obtained for CH_2Cl_2 glasses at 77K. Asterisk denotes a signal derived presumably from the dicationic species.

https://doi.org/10.1021/acsorginorgau.4c00021
ACS Org. Inorg. Au 2024, 4, 504−516

Compounds with $0 < \Gamma < 0.5$ are categorized as Class II, while those with $\Gamma > 0.5$ are categorized as Class III. The Γ values for the four complexes exceed 0.5 in the order of $[\mathbf{1}^{\mathbf{RuNi}}]^{+\bullet} > [\mathbf{1}^{\mathbf{RuZn}}]^{+\bullet} > [\mathbf{1}^{\mathbf{FeZn}}]^{+\bullet} > [\mathbf{1}^{\mathbf{FeNi}}]^{+\bullet}$. On the basis of these results, their electronic couplings V_{ab} evaluated as Class III compounds are 2175 ($[\mathbf{1}^{\mathbf{FeZn}}]^{+\bullet}$), 2605 ($[\mathbf{1}^{\mathbf{RuZn}}]^{+\bullet}$), 1692 ($[\mathbf{1}^{\mathbf{FeNi}}]^{+\bullet}$), and 2457 cm^{-1} ($[\mathbf{1}^{\mathbf{RuNi}}]^{+\bullet}$). Negligible solvent dependence of the IVCT bands for nickel complex $[\mathbf{1}^{\mathbf{MNi}}]^{+\bullet}$ further provides a proof of the assignment as "Class III" (Figure S1),[85,86] although slight changes of the absorption spectra of $[\mathbf{1}^{\mathbf{FeNi}}]^{+\bullet}$ indicate its Class II/III character. This assignment is also supported by the ESR and DFT studies discussed below. The solvent-dependent nature of the IVCT bands of zinc complexes $[\mathbf{1}^{\mathbf{MZn}}]^{+\bullet}$ could be rationalized by the coordination of the solvent molecule to the central zinc atom, which perturbs the electronic structures of the metalloporphyrin-containing bridging ligands (*vide infra*).

Comparison of V_{ab} values between the iron and ruthenium complexes should be made with caution. Ruthenium MV complexes generally exhibit stronger BL radical characters, and the three-state model, which considers the oxidation states of both of the metal fragments and the BL, has been frequently used for analysis of IVCT bands. The V_{ab} values obtained using the two-state Hush analysis may deviate from those obtained by the three-state model to some extent. Iron MV complexes, on the other hand, tend to show metal-localized character and the two-state Hush model can be appropriately used. The trend of the V_{ab} values, i.e. Ru complexes > Fe complexes and Zn complexes > Ni complexes, happen to be coincident with the trends in charge delocalization obtained by the DFT study (vide infra). When compared to the dinuclear Ru derivatives with the free-base (2643 cm^{-1}) and the MnCl porphyrin derivatives (2551 cm^{-1}), the V_{ab} value of $[\mathbf{1}^{\mathbf{RuZn}}]^{+\bullet}$ falls between them.[75,77] This result clearly revealed the charge-delocalized properties of the porphyrin-containing organometallic molecular wires can be controlled successfully by the metals in the termini and the porphyrin moieties.

iii) ESR Spectroscopy. ESR studies were performed for the monocationic radical species $[\mathbf{1}^{\mathbf{MM'}}]^{+\bullet}$ (CH_2Cl_2 glasses at 77 K; Figure 7 and Table 4). Isotropic signals were observed for the ruthenium complexes $[\mathbf{1}^{\mathbf{RuZn}}]^{+\bullet}$ and $[\mathbf{1}^{\mathbf{RuNi}}]^{+\bullet}$, suggesting localization of the radicals on the BLs. While the iron−zinc complex $[\mathbf{1}^{\mathbf{FeZn}}]^{+\bullet}$ showed a signal with slight anisotropic features, the other iron−nickel complex $[\mathbf{1}^{\mathbf{FeNi}}]^{+\bullet}$ showed a clearly anisotropic signal indicating substantial metal-centered radical character. Because the mono- and dinuclear radical species with the FeCp*(dppe) fragments commonly show anisotropic *g*-tensors,[37,87−89] the weak anisotropic signal observed for $[\mathbf{1}^{\mathbf{FeZn}}]^{+\bullet}$ indicates significant delocalization of the radical over the porphyrin moiety in the MV complexes.

Table 4. ESR Parameters for $[\mathbf{1}^{\mathbf{MM'}}]^{+\bullet}$[a]

	g_1	g_2	g_3	g_{iso}
$[\mathbf{1}^{\mathbf{FeZn}}]^{+\bullet}$	2.007	2.036	2.068	2.037
$[\mathbf{1}^{\mathbf{RuZn}}]^{+\bullet}$	2.031	-	-	-
$[\mathbf{1}^{\mathbf{FeNi}}]^{+\bullet}$	1.998	2.063	2.223	2.094
$[\mathbf{1}^{\mathbf{RuNi}}]^{+\bullet}$	2.043	-	-	-

[a]Recorded as CH_2Cl_2 glasses at 77K

DFT Calculations

In order to get insight into the trends of the electronic interactions between the two metal termini DFT calculations were performed for the simplified neutral ($\mathbf{1'}^{\mathbf{MM'}}$) and monocationic species ($[\mathbf{1'}^{\mathbf{MM'}}]^{+\bullet}$), where the aryl groups were replaced by the phenyl groups ('-series).

The geometries of the model neutral complexes $\mathbf{1'}^{\mathbf{MM'}}$ were optimized at the B3LYP/LanL2DZ (for the transition metals) and 6-31G(d) (for the others) levels of theory (Figure 8). Both

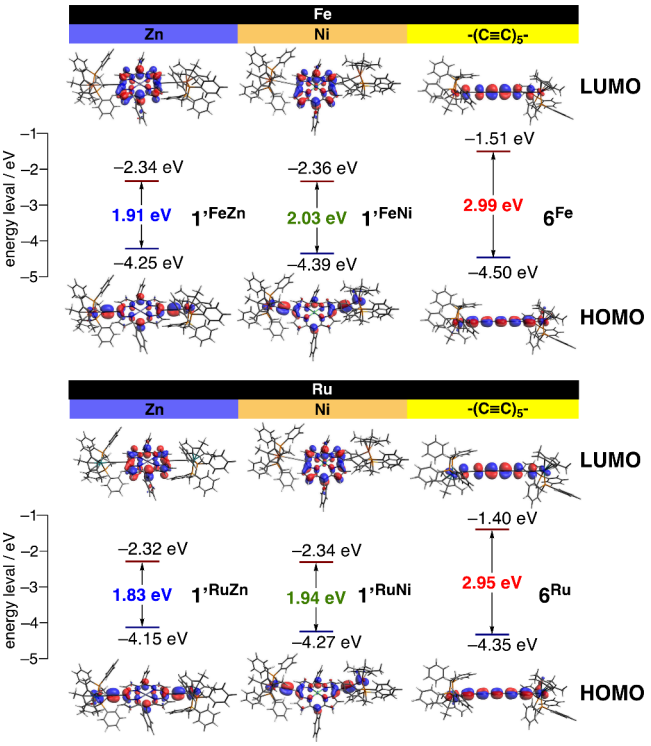

Figure 8. Frontier orbitals of $\mathbf{1'}^{\mathbf{MM'}}$ and $\mathbf{6}^{\mathbf{M}}$ calculated by the DFT method (B3LYP/LanL2DZ,6-31G(d),CPCM(CH_2Cl_2)).

of the Zn complexes $\mathbf{1'}^{\mathbf{FeZn}}$ and $\mathbf{1'}^{\mathbf{RuZn}}$ are planar, whereas the Ni derivatives $\mathbf{1'}^{\mathbf{FeNi}}$ and $\mathbf{1'}^{\mathbf{RuNi}}$ are distorted from the planarity as observed for the solid-state structure of $\mathbf{1}^{\mathbf{RuNi}}$. The highest occupied molecular orbitals (HOMOs) and the lowest unoccupied molecular orbitals (LUMOs) of the four complexes $\mathbf{1'}^{\mathbf{MM'}}$ are quite similar to each other. The HOMOs of $\mathbf{1'}^{\mathbf{MM'}}$ bearing the dπ-pπ character are fully delocalized over the M-porphyrin(M')-M linkage, while the virtually degenerate LUMOs and LUMO+1's are mainly composed of the porphyrin e_{gx}- and e_{gy}-type orbitals. It is noted that the contributions of the Zn and Ni atoms embedded in the porphyrins to the frontier orbitals are negligible. Due to the planar geometry for the Zn porphyrin derivatives $\mathbf{1'}^{\mathbf{MZn}}$, their HOMO−LUMO gaps (1.91 eV ($\mathbf{1}^{\mathbf{FeZn}}$), 1.83 eV ($\mathbf{1}^{\mathbf{RuZn}}$)) are slightly smaller than those of the Ni complexes $\mathbf{1}^{\mathbf{MNi}}$ (2.03 eV ($\mathbf{1}^{\mathbf{FeNi}}$), 1.94 eV ($\mathbf{1}^{\mathbf{RuNi}}$)). Furthermore, the HOMO energies of the Zn porphyrin complexes $\mathbf{1'}^{\mathbf{MZn}}$ are higher than those of the Ni complexes $\mathbf{1'}^{\mathbf{MNi}}$. These properties render the MV complexes more localized on the BLs in accord with the experimental results.

For comparison, we have also made calculations to examine the influence of the metal ion for decapentayne-diyl complexes $\mathbf{6}^{\mathbf{M}}$ with the iron and ruthenium termini, $[\mu$-$(C{\equiv}C)_5][MCp^*$-$(dppe)]_2$ (M= Fe, Ru), where the metal−metal distances

https://doi.org/10.1021/acsorginorgau.4c00021
ACS Org. Inorg. Au 2024, 4, 504−516

(∼1.54 nm) are similar to those of $\mathbf{1}^{\mathbf{MM'}}$ (1.54−1.63 nm). Both of the HOMOs and LUMOs of $\mathbf{6}^{\mathbf{M}}$ contain the dπ-pπ orbitals spreading over the M-$(C{\equiv}C)_5$-M frameworks. The HOMO energies of $\mathbf{6}^{\mathbf{M}}$ are slightly lower than those of $\mathbf{1}^{\mathbf{MM'}}$ by 0.10−0.25 eV, whereas the LUMO energies of $\mathbf{6}^{\mathbf{M}}$ are significantly higher than those of $\mathbf{1}^{\mathbf{MM''}}$, leading to the comparatively large HOMO−LUMO gaps ($\mathbf{6}^{\mathbf{Fe}}$: 2.99 eV, $\mathbf{6}^{\mathbf{Ru}}$: 2.95 eV).

To consider the differences and estimate the energy levels of the frontier orbitals of the π- and *d*-systems of the metal and linker fragments the hydrogen-terminated derivatives of the metal fragments (**M-H**) and the linkers (**MP** and $\mathbf{C_{10}H_2}$) were subjected to calculation, and the results are summarized in Figure 9 and Figure S2. While the LUMO levels for **MP**s and

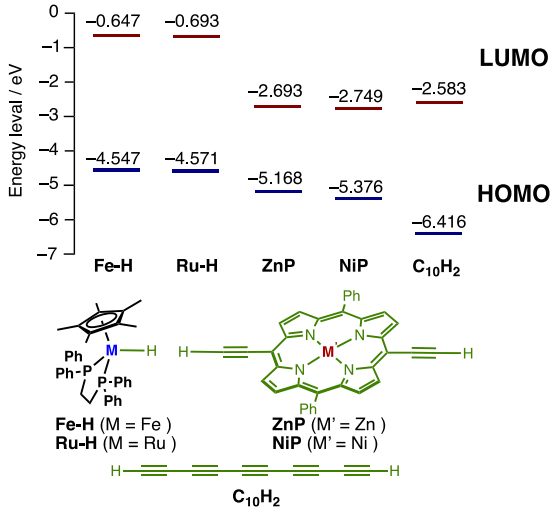

Figure 9. Energy diagrams for the models of the fragments of $\mathbf{1}^{\mathbf{MM'}}$.

$\mathbf{C_{10}H_2}$ are similar, the HOMO of $\mathbf{C_{10}H_2}$ is lower in energy than those of **MP**s to lead to the smaller HOMO−LUMO gaps for **MP**s, in accord with our expectation as demonstrated in Figure 1. The HOMOs of **M-H**s lying between the HOMOs and LUMOs of **MP** and $\mathbf{C_{10}H_2}$ ligands and closer to the HOMOs of **MP**s as well should lead to (1) effective back-donating pπ-dπ orbital interactions (see the HOMOs of $\mathbf{1}^{\mathbf{MM'}}$) and (2) the small contribution of the metal fragments to the LUMOs.

Spin distributions of the monocationic MV complexes were calculated to get insight into the extent of the charge delocalization. For the sake of simplicity, calculations were made for another truncated system (”-series; cf. the above-mentioned ’-series), wherein the dppe and Cp* ligands and the *t*-butyl groups were substituted with dmpe (1,2-dimethylphosphinoethane) and η^5-C_5H_5 ligands and hydrogen atoms, respectively (Figure 10). For $[\mathbf{1}^{\mathbf{FeZn}}]^{+\bullet}$ and $[\mathbf{1}^{\mathbf{RuM'}}]^{+\bullet}$, the spin densities are spread across the M-porphyrin(M’)-M linkages with equal spin densities on the terminal iron and ruthenium fragments. By contrast, the spin density of the iron−nickel species $[\mathbf{1}^{\mathbf{FeNi}}]^{+\bullet}$ is distributed unsymmetrically, suggesting Class II nature as is consistent with the experimental results. In the iron derivatives $[\mathbf{1}^{\mathbf{FeM'}}]^{+\bullet}$, the spin density is predominantly localized on the iron atoms ($[\mathbf{1}^{\mathbf{FeZn}}]^{+\bullet}$: 0.52 e; $[\mathbf{1}^{\mathbf{FeNi}}]^{+\bullet}$: 0.74 e), whereas that of the ruthenium derivatives $[\mathbf{1}^{\mathbf{RuM'}}]^{+\bullet}$ is more localized on the bridging ligand as indicated by the spin densities on the metal fragments ($[\mathbf{1}^{\mathbf{RuZn}}]^{+\bullet}$: 0.32 e; $[\mathbf{1}^{\mathbf{RuNi}}]^{+\bullet}$: 0.35 e). No apparent spin density is found on the Zn and Ni atoms, indicating that the central metal atoms in the porphyrins do not directly participate in the electronic interactions between the two metal ends but rather control the conformation and electron density of the porphyrin core.

The simplified decapentayne-diyl complexes $[\mathbf{6}^{\mathbf{M}}]^{+\bullet}$, $[\mu$-$(C{\equiv}C)_5][M(\eta^5$-$C_5H_5)(dmpe)]_2$ (M = Fe, Ru), were examined for comparison. The features of the spin density distribution are quite similar to those of $[\mathbf{1}^{\mathbf{MNi}}]^{+\bullet}$, i.e. the spin densities of the iron ($[\mathbf{6}^{\mathbf{Fe}}]^{+\bullet}$) and ruthenium derivatives ($[\mathbf{6}^{\mathbf{Ru}}]^{+\bullet}$) are more localized on the terminal metal fragments and the bridging moieties, respectively. This result, in turn, indicates that the charge-delocalizing abilities of the decapentayne and diethynyl-nickelporphyrin bridges are comparable. Furthermore, charge-delocalization on $[\mathbf{1}^{\mathbf{FeZn}}]^{+\bullet}$ is more evenly distributed over the backbone than that on $[\mathbf{1}^{\mathbf{RuZn}}]^{+\bullet}$. In contrast, the reported dinuclear MV complexes featuring the FeCp*(dppe) fragments with molecular lengths exceeding 1.5 nm exhibit Class II charge-localized states,[43,89] the porphyrin linkers turn out to cause the extensive charge-delocalization due to their smaller HOMO−LUMO gaps.

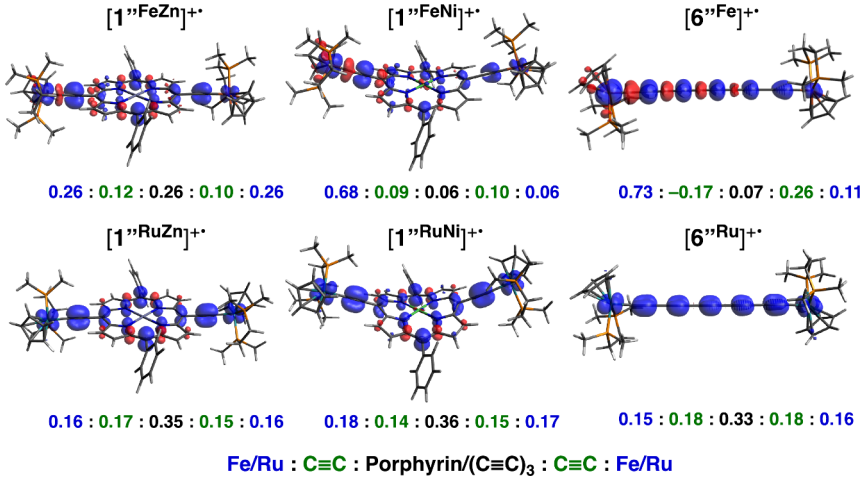

Figure 10. Spin density plots and spin densities of $[\mathbf{1}^{\mathbf{MM'}}]^{+\bullet}$ and $[\mathbf{6}^{\mathbf{M}}]^{+\bullet}$ calculated by the DFT method (UB3LYP/LanL2DZ,6-31G(d),CPCM(CH_2Cl_2)).

https://doi.org/10.1021/acsorginorgau.4c00021
ACS Org. Inorg. Au 2024, 4, 504−516

Modulating Electron Transfer Property by Nitrogen Donor

The solvent-dependence of the IVCT bands of the zinc complexes $[\mathbf{1}^{\mathbf{MZn}}]^{+\bullet}$ mentioned above could be ascribed to coordination of solvent molecules to the axial sites of the metalloporphyrin units, suggesting the possibility to modulate the metal−metal interaction by donor molecules. Then we examined addition effects of nitrogen donors on the wirelike behavior, i.e. the metal−metal interactions, of $[\mathbf{1}^{\mathbf{MZn}}]^{+\bullet}$.[90]

When pyridine was added to a CH_2Cl_2 solution of $[\mathbf{1}^{\mathbf{FeZn}}]^{+\bullet}$, the IVCT band was shifted to longer wavelength (from 2298 to 2465 nm; Figure 11). Formation of a 1:1 adduct $[\mathbf{1}^{\mathbf{FeZn}}]^{+\bullet}$

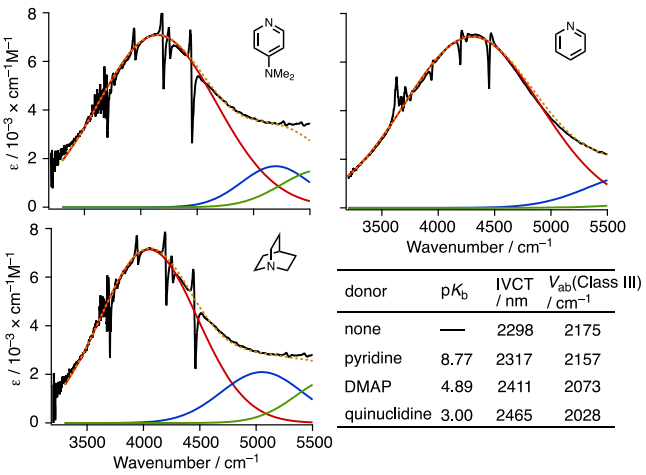

donor	pK_b	IVCT / nm	V_{ab}(Class III) / cm^{-1}
none	—	2298	2175
pyridine	8.77	2317	2157
DMAP	4.89	2411	2073
quinuclidine	3.00	2465	2028

Figure 11. NIR spectra for the adducts of $[\mathbf{1}^{\mathbf{FeZn}}]^{+\bullet}$ and various *N*-donors (observed in CH_2Cl_2) and their deconvoluted spectra. Five equivalents of the donors were added. V_{ab} was calculated from the Hush formula for Class III species.

pyridine was confirmed by ESI-MS and elemental analysis of the isolated product.[91] More prominent bathochromic shifts of the IVCT bands were brought about by addition of quinuclidine (2465 nm) and DMAP (2411 nm), leading to the electronic coupling (V_{ab}) of 2028 and 2073 cm^{-1}, respectively. These results imply that the metal−metal interaction, i.e. wirelike performance, is weakened by the coordination of the nitrogen donors in the order of pyridine < DMAP < quinuclidine. This order turns out to be correlated to the decreasing order of the pK_b values, which can be correlated to the σ-donation ability of the donor nitrogen atom, i.e. a stronger Lewis base causes larger red shifts of the IVCT bands (weaker interaction).[18] Coordination of electron-donating ligands to the zinc center would destabilize the HOMO levels of the metalloporphyrin parts to facilitate the charge-delocalization of the MV complexes,[92,32] as also supported by our preliminary DFT study (Figure S4).[93] However, the observed results contradict this expectation. Although further investigation is required, this observation discussed above might be ascribed to a change of the planarity of the porphyrin ring brought about by the ligation of donors. The ring distortion from the planarity would lead to a decrease of the degree of π-conjugation to suppress the electronic communication. Thus, the strength of the electronic communication can be slightly weakened by the addition of appropriate donors.

CONCLUSIONS

A series of electron-rich dinuclear organometallic complexes with the diethynylated metalloporphyrin linkers ($\mathbf{1}^{\mathbf{MM'}}$) and their 1e-oxidized monocation radical species ($[\mathbf{1}^{\mathbf{MM'}}]^{+\bullet}$) have been prepared and characterized with the focus on their wirelike behavior, i.e. the metal−metal interaction in $[\mathbf{1}^{\mathbf{MM'}}]^{+\bullet}$. The IVCT bands and DFT calculations reveals that, despite the long metal−metal separation of 1.5 nm, the molecular wires exhibit the strong metal−metal interaction, i.e. $\mathbf{1}^{\mathbf{MM'}}$ serve as efficient long molecular wires. According to the DFT calculations, the excellent wirelike behavior can be ascribed to the MOs of the metalloporphyrin linker moieties being closer in energy to those of the terminal metal fragments to lead to efficient π-conjugation over the organometallic wires. Furthermore, the wirelike behavior can be tuned by the addition of nitrogen donors, potentially leading to switching systems in molecular electronics.

EXPERIMENTAL SECTION

General Procedures and Reagents

Reactions were performed under N_2 atmosphere using standard Schlenk tube techniques unless stated otherwise. THF, CH_2Cl_2, diethyl ether, pentane were purchased from Kanto chemical Co Inc. purified by the Grubbs solvent system.[94] Dry MeOH and benzene purchased from Kanto chemical Co Inc. were used as received. [5,15-bis(ethynyl)-10,20-bis(3,5-di(*tert*-butyl)phenyl)porphinato]zinc(II) $\mathbf{3}^{\mathbf{Zn}}$,[95−97] [5,15-bis(ethynyl)-10,20-bis(3,5-di(*tert*-butyl)phenyl)-porphinato]nickel(II) $\mathbf{3}^{\mathbf{Ni}}$,[98] $\mathbf{4}^{\mathbf{Fe}}$,[52] $\mathbf{4}^{\mathbf{Ru}}$,[52] FeCp*(dppe)Cl,[99,100] and RuCp*(dppe)Cl[101,102] were prepared according to the reported procedures. Triethylamine was predried over NaOH and distilled from CaH_2. Other regents were used as received. Silica gel (Kanto chemical Co Inc. Silica Gel 60N) and alumina (Merck Alminium oxide 90 standardized) were used as received.

NMR spectra were recorded on a JEOL-JMN-EX-300 MHz (^{1}H NMR 300 MHz, ^{31}P NMR 121.5 MHz). Solvents for NMR measurements were dried over molecular sieves, degassed, and stored under nitrogen. Chemical shifts (downfield from TMS (^{1}H, ^{13}C) and H_3PO_4 (^{31}P)) and coupling constants are reported in ppm and in Hz, respectively. IR and UV−vis-near IR spectra were recorded on JASCO FT/IR 4200 and JASCO V-670 spectrometers, respectively. Electrochemical measurements were made with a BAS 100B/W analyzer (observed in CH_2Cl_2; [complex] = ca. 1×10^{-3} M; $[NBu_4PF_6]$ = 0.1 M; working electrode: Pt (circular shape with a radius of 1.6 mm.), counter electrode: Pt, reference electrode: Ag/$AgNO_3$; scan rate was 100 mV/s, initial potentials were set to open circuit potentials, at 298 K). Before the measurements, the working electrode was polished with diamond (1 μm) and alumina (0.05 μm). After the measurements, ferrocene (Fc) was added to the mixture and the potentials were calibrated with respect to the $Fc/Fc^{+\bullet}$ redox couple. ESR spectra were obtained on a JES-FA200 spectrometer. Elemental analyses were performed at the Center for Advanced Materials Analysis, Technical Department, Tokyo Institute of Technology. X-ray crystal analysis was performed on a Bruker Smart Apex II Ultra diffractometer.

Preparation of $\mathbf{1}^{\mathbf{MM'}}$

FeCp*(dppe) Zn(II) Porphyrin Complex $\mathbf{1}^{\mathbf{FeZn}}$. To a mixture of FeCp*(dppe)Cl (750 mg, 1.2 mmol) and KPF_6 (265 mg, 1.4 mmol) dissolved in MeOH (32 mL)-THF (8 mL) was added $\mathbf{3}^{\mathbf{Zn}}$ (240 mg, 0.30 mmol), and the resultant mixture was stirred for 48 h at room temperature. Then the organic solvent was removed under reduced pressure, and the resultant residue was extracted with CH_2Cl_2 and filtered through a Celite pad. The filtrate was concentrated *in vacuo* to afford the iron vinylidene intermediate as a black solid, which was dissolved in CH_2Cl_2 (16 mL). DBU (0.96 mL, 0.66 mmol) was added to the obtained CH_2Cl_2 solution, and the mixture was stirred for 3 h. The volatiles were removed under reduced pressure, and the residue was washed with MeOH (20 mL) three times. The resulting black solid was extracted with benzene and filtered through a Celite pad. Removal of the volatiles under reduced pressure afforded $\mathbf{1}^{\mathbf{FeZn}}$ (367 mg, 0.19 mmol, 62% yield) as a black solid. IR (KBr/cm^{-1}): 1992 ν(C≡C). ^{1}H NMR (300 MHz, C_6D_6, rt): δ 8.92 (br, β-CH, 4H),

https://doi.org/10.1021/acsorginorgau.4c00021
ACS Org. Inorg. Au 2024, 4, 504−516

8.64 (br, β-CH, 4H), 8.06−8.25 (m, o-ArH and dppe-Ph, 12H), 7.89 (s, p-ArH, 2H), 7.39−7.52, 7.10−7.18, 6.90−6.94 (m, dppe-Ph, 32H), 3.15 (m, dppe-CH_2, 4H), 2.06 (m, dppe-CH_2, 4H), 1.75 (s, C_5Me_5, 30H), 1.50 (s, *t*-Bu, 36H). ^{31}P NMR (121.5 MHz, C_6D_6, rt): δ 101.3 (s, dppe). MS(ESI) *m/z*: Calcd. For $C_{124}H_{129}Fe_2N_4P_4Zn$ 1974 $[M + H]^+$, Found: 1974. Anal. Calcd. for $C_{125.1}H_{130.2}Cl_{2.2}Fe_2N_4P_4Zn$ ($\mathbf{1}^{\mathbf{FeZn}}\bullet(CH_2Cl_2)_{1.1}$): C, 72.63, H, 6.34, N, 2.71. Found: C, 72.46, H, 6.82, N, 2.91.

RuCp*(dppe) Zn(II) Porphyrin Complex $\mathbf{1}^{\mathbf{RuZn}}$. To a CH_2Cl_2 (30 mL) solution of RuCp*(dppe)Cl (804 mg, 1.2 mmol) was added AgOTf (274 mg, 1.1 mmol), and the resultant mixture was stirred for 20 min at room temperature. Then, $\mathbf{3}^{\mathbf{Zn}}$ (240 mg, 0.30 mmol) was added, and the resulting mixture was stirred for 3 h at room temperature. The obtained mixture was filtered through a Celite pad and eluted with CH_2Cl_2. The filtrate was concentrated *in vacuo* to give the ruthenium vinylidene intermediate as a black solid. To the black solid dissolved in CH_2Cl_2 (20 mL) solution was added DBU (0.18 mL, 1.2 mmol), and the mixture was stirred for 3 h. The volatiles were removed under reduced pressure to leave a residue, which was washed with MeOH (20 mL) three times. The resulting black solid was extracted with benzene and passed through a Celite pad. The filtrate was concentrated in vacuo, and the obtained solid was crystallized from CH_2Cl_2/hexane to give $\mathbf{1}^{\mathbf{RuZn}}$ (180 mg, 0.087 mmol, 29% yield) as black crystals. IR (KBr/cm^{-1}): 2021 ν(C≡C). ^{1}H NMR (300 MHz, C_6D_6, rt): δ 9.01 (d, J = 4.2 Hz, porphyrin β-CH, 4H), 8.74 (d, J = 4.2 Hz, porphyrin β-CH, 4H), 7.95−8.20 (m, *o*-ArH and dppe-Ph, 12H), 7.94 (s, *p*-ArH, 2H), 6.83−7.26 (m, dppe-Ph, 32H), 3.20−3.24 (m, dppe-CH_2, 4H), 2.19−2.22 (m, dppe-CH_2, 4H), 1.87 (s, C_5Me_5, 30H), 1.55 (s, *t*-Bu, 36H). ^{31}P NMR (121.5 MHz, C_6D_6, rt): δ 82.6 (s, dppe). MS(ESI) *m/z*: Calcd. For $C_{124}H_{128}Ru_2N_4P_4Zn$ 2065 $[M]^+$, Found: 2065. Anal. Calcd. for $C_{127}H_{134}Cl_6N_4P_4Ru_2Zn$ ($\mathbf{1}^{\mathbf{RuZn}}\bullet(CH_2Cl_2)_3$): C, 65.73, H, 5.82, N, 2.41. Found: C, 65.78, H, 5.59, N, 2.28. HRMS(ESI, CsI) *m/z*: $[M + H]^+$ Calcd for $C_{124}H_{129}N_4P_4Ru_2Zn$ 2065.6546, Found: 2065.6544.

FeCp*(dppe) Ni(II) Porphyrin Complex $\mathbf{1}^{\mathbf{FeNi}}$. To a mixture of FeCp* (dppe)Cl (394 mg, 0.630 mmol, 5.0 equiv) and KPF_6 (127 mg, 0.203 mmol, 5.6 equiv) dissolved in MeOH (15 mL)-THF (5 mL) was added $\mathbf{3}^{\mathbf{Ni}}$ (98.5 mg, 0.124 mmol), and the resultant mixture was stirred for 48 h at room temperature. Then the volatiles were removed under reduced pressure, and the obtained residue was extracted with CH_2Cl_2 and filtered through a Celite pad. The filtrate was concentrated in vacuo to afford the iron vinylidene intermediate as a black solid, which was dissolved in CH_2Cl_2 (8 mL). Then DBU (82 mL, 0.548 mmol) was added to the CH_2Cl_2 solution, and the resultant mixture was stirred for 4 h. After removal of the volatiles under reduced pressure, the obtained residue was dissolved in benzene, and the product was precipitated by addition of methanol. The obtained solid was washed with methanol and diethyl ether successively to afford $\mathbf{1}^{\mathbf{FeNi}}$ (82.4 mg, 0.0422 mmol, 34% yield) as a black solid. IR (KBr/cm^{-1}) 2013 ν(C≡C). ^{1}H NMR (300 MHz, C_6D_6, r.t.): δ 8.88 (br, β-CH, 4H), 8.40 (br, β-CH, 4H), 8.05−8.20 (m, dppe-Ph, 8H), 7.95 (d, J = 1.2 Hz, *o*-ArH, 4H), 7.79 (t, J = 1.2 Hz, *p*-ArH, 2H), 6.80−7.48 (m, dppe-Ph, 32H), 3.07 (m, dppe-CH_2, 4H), 2.02 (m, dppe-CH_2, 4H), 1.62 (s, C_5Me_5, 30H), 1.42 (s, *t*-Bu, 36H). ^{31}P NMR (121.5 MHz, C_6D_6, r.t.) δ 100.7. Anal. Calcd. for $C_{124.5}H_{130}ClN_4P_4Fe_2Ni$ ($\mathbf{1}^{\mathbf{FeNi}}\bullet(CH_2Cl_2)_{0.5}$): C, 74.35, H, 6.47, N, 2.79. Found: C, 74.37, H, 6.57, N, 2.83. HRMS (ESI, CsI) *m/z*: $[M]^+$ Calcd. for $C_{124}H_{129}N_4P_4Fe_2Ni$ 1967.7273. Found 1967.7277.

RuCp*(dppe) Ni Porphyrin Complex $\mathbf{1}^{\mathbf{RuNi}}$. To a CH_2Cl_2 (20 mL) solution of RuCp*(dppe)Cl (350 mg, 0.375 mmol, 2.5 equiv) was added $AgPF_6$ (91.3 mg, 0.361 mmol, 2.4 equiv), and the resultant mixture was stirred at room temperature. After 20 min, the resulting mixture containing $[RuCp^*(dppe)]PF_6$ was added to a CH_2Cl_2 (50 mL) solution of $\mathbf{3}^{\mathbf{Ni}}$ via cannula, and the resulting mixture was stirred for 11 h at room temperature. The reaction mixture was concentrated in vacuo and the residue was extracted with CH_2Cl_2 and filtered through a Celite pad. The filtrate was concentrated in vacuo to give the ruthenium vinylidene intermediate as a black solid, which was dissolved in CH_2Cl_2 (8 mL). To the obtained solution was added DBU (67.3 μL, 0.450 mmol), and the resultant mixture was stirred for 3 h. Then the volatiles were removed under reduced pressure, and the obtained residue was washed with MeOH. The resulting black solid was dissolved in benzene, and the product was precipitated by addition of methanol. The residue was washed with methanol and diethyl ether successively to give $\mathbf{1}^{\mathbf{RuNi}}$ (82.7 mg, 0.0402 mmol, 27% yield) as a dark green solid. Crystals suitable for X-ray analysis were obtained by slow diffusion of diethyl ether into a CH_2Cl_2 solution of $\mathbf{1}^{\mathbf{RuNi}}$. IR (KBr): 2034 cm^{-1} ν(RC≡CRu). ^{1}H NMR (400 MHz, C_6D_6, r.t.) δ 8.78 (d, J = 3.6 Hz, β-CH, 4H), 8.55 (d, J = 3.6 Hz, β-CH, 4H), 7.99 (d, J = 1.8 Hz, *o*-ArH, 4H), 7.93−8.35 (m, dppe-Ph, 40H), 7.82 (t, J = 1.8 Hz, *p*-ArH, 2H), 7.25−7.34, 7.13−7.24,7.05−7.10, 6.91−7.00 (m, dppe-Ph, 32H), 3.10 (m, dppe-CH_2, 4H), 2.09 (m, dppe-CH_2, 4H), 1.79 (s, C_5Me_5, 30H), 1.43 (s, *t*-Bu, 36H). ^{31}P NMR (161.9 MHz, C_6D_6, r.t.) δ 82.3. Anal. Calcd. for $C_{125.3}H_{131.6}Cl_{2.6}N_4NiP_4Ru_2$ ($\mathbf{1}^{\mathbf{RuNi}}\bullet(CH_2Cl_2)_{1.3}$): C, 69.37, H, 6.07, N, 2.58. Found: C, 69.13, H, 6.55, N, 2.56. HRMS (ESI, CsI) *m/z*: $[M]^+$ Calcd. for $C_{124}H_{129}N_4P_4Fe_2Ni$ 2058.6561, Found: 2058.6567 $[M]^+$.

Theoretical Calculations

DFT calculations were performed by using the Gaussian 16 (C03) program package.[103] Optimizations of the geometries and the single point calculations of $\mathbf{1}^{\mathbf{MM'}}$, $\mathbf{6}^{\mathbf{M}}$, $[\mathbf{1}^{\mathbf{"MM'"}}]^{+\bullet}$, $[\mathbf{6}^{\mathbf{"M"}}]^{+\bullet}$ were carried out at the (U)B3LYP/LanL2DZ levels of theory with the CPCM solvent continuum model (CH_2Cl_2). In the optimized geometry, no imaginary vibrational frequency was found for the vibrational frequency analysis. We also performed DFT calculations of $[\mathbf{1}^{\mathbf{"MM'"}}]^{+\bullet}$ at the UBLYP35/Def2-SVP level of theory with the CPCM solvent continuum (CH_2Cl_2),[104] known for its reliable theoretical MV predictions. However, the results obtained suggested that the spin density was localized on the Ni and Zn atoms in the porphyrins, contradicting the experimental findings

■ ASSOCIATED CONTENT

Data Availability Statement

The data underlying this study are available in the published article and its Supporting Information.

Supporting Information

The Supporting Information is available free of charge at https://pubs.acs.org/doi/10.1021/acsorginorgau.4c00021.

> Preparation of cationic complexes; solvent dependent NIR spectra of $[\mathbf{1}^{\mathbf{FeNi}}]^{+\bullet}$ and $[\mathbf{1}^{\mathbf{RuNi}}]^{+\bullet}$, frontier orbitals of **M-H**, **M'P**, and $\mathbf{C_{10}H_2}$; NMR spectra for $\mathbf{1}^{\mathbf{FeZn}}$. $\mathbf{1}^{\mathbf{RuZn}}$, $\mathbf{1}^{\mathbf{FeNi}}$, $\mathbf{1}^{\mathbf{RuNi}}$, $\mathbf{4}^{\mathbf{Fe}}$, and $\mathbf{4}^{\mathbf{Ru}}$; crystal data and structure refinement for $\mathbf{1}^{\mathbf{RuNi}}$; Cartesian coordinates of $\mathbf{1'}^{\mathbf{FeZn}}$, $\mathbf{1'}^{\mathbf{RuZn}}$, $\mathbf{1'}^{\mathbf{FeNi}}$, $\mathbf{1'}^{\mathbf{RuNi}}$, $\mathbf{6}^{\mathbf{Fe}}$, $\mathbf{6}^{\mathbf{Ru}}$, $[\mathbf{1}^{\mathbf{"FeZn"}}]^{+\bullet}$, $[\mathbf{1}^{\mathbf{"RuZn"}}]^{+\bullet}$, $[\mathbf{1}^{\mathbf{"FeNi"}}]^{+\bullet}$, $[\mathbf{1}^{\mathbf{"RuNi"}}]^{+\bullet}$, $[\mathbf{6}^{\mathbf{"Fe"}}]^{+\bullet}$, and $[\mathbf{6}^{\mathbf{"Ru"}}]^{+\bullet}$ (PDF)

Accession Codes

CCDC 2343973 contains the supplementary crystallographic data for this paper. These data can be obtained free of charge via www.ccdc.cam.ac.uk/data_request/cif, or by emailing data_request@ccdc.cam.ac.uk, or by contacting The Cambridge Crystallographic Data Centre, 12 Union Road, Cambridge CB2 1EZ, UK; fax: +44 1223 336033.

■ AUTHOR INFORMATION

Corresponding Author

Munetaka Akita − *Laboratory for Chemistry and Life Science, Institute of Innovative Research, Tokyo Institute of Technology, Yokohama 226-8503, Japan;* orcid.org/0000-0001-7007-9621; Email: akitatit@icloud.com; Fax: (+81)45-924-5230

https://doi.org/10.1021/acsorginorgau.4c00021
ACS Org. Inorg. Au 2024, 4, 504−516

Authors

Masahito Murai − *Laboratory for Chemistry and Life Science, Institute of Innovative Research, Tokyo Institute of Technology, Yokohama 226-8503, Japan;* Present Address: Present Address: Department of Chemistry, Graduate School of Science, and Integrated Research Consortium on Chemical Sciences (IRCCS), Nagoya University, Furo, Chikusa, Nagoya, 464−8602, Japan

Masanori Ono − *Laboratory for Chemistry and Life Science, Institute of Innovative Research, Tokyo Institute of Technology, Yokohama 226-8503, Japan*

Yuya Tanaka − *Laboratory for Chemistry and Life Science, Institute of Innovative Research, Tokyo Institute of Technology, Yokohama 226-8503, Japan;* orcid.org/0000-0002-0674-660X

Complete contact information is available at: https://pubs.acs.org/10.1021/acsorginorgau.4c00021

Author Contributions

CRediT: **Masahito Murai** conceptualization, data curation, formal analysis, investigation, writing-original draft; **Masanori Ono** data curation, formal analysis, investigation; **Yuya Tanaka** data curation, formal analysis, funding acquisition, investigation, writing-original draft, writing-review & editing; **Munetaka Akita** conceptualization, funding acquisition, investigation, supervision, writing-review & editing.

Notes

The authors declare no competing financial interest.

■ ACKNOWLEDGMENTS

This work was supported by the JSPS KAKENHI Grant Number 26810031 (MA) and 21K05211 (YT). Theoretical calculations were performed using computers at the Research Center for Computational Science, Okazaki, Japan (23-IMS-C063, 24-IMS-C060). This work was performed under the Cooperative Research Program of "Network Joint Research Center for Materials and Devices." We are grateful to the three former group members, Dr. Takashi Koike, Ms. Keiko Fukuda, Mr. Reo Kawano. for their assistance with synthesis and discussion. We thank Dr. Takayuki Kamihara of the Center for Advanced Materials Analysis, Technical Department, Tokyo Institute of Technology, for the assistance with analysis of the NMR data. We also thank Ms. Keiko Ideta (Kyushu Univ.) and Dr. Atushi Tahara (Tohoku Univ.) for the help of ESR measurements.

■ REFERENCES

(1) Richardson, D. E.; Taube, H. Mixed-Valence Molecules: Electronic Delocalization and Stabilization. *Coord. Chem. Rev.* **1984**, *60*, 107−129.

(2) Ward, M. D. Metal-Metal Interactions in Binuclear Complexes Exhibiting Mixed Valency; Molecular Wires and Switches. *Chem. Soc. Rev.* **1995**, *24* (2), 121−134.

(3) Demadis, K. D.; Hartshorn, C. M.; Meyer, T. J. The Localized-to-Delocalized Transition in Mixed-Valence Chemistry. *Chem. Rev.* **2001**, *101* (9), 2655−2686.

(4) Bernhardt, P. V.; Bozoglián, F.; Macpherson, B. P.; Martínez, M. Molecular Mixed-Valence Cyanide Bridged Co^{III}−Fe^{II} Complexes. *Coord. Chem. Rev.* **2005**, *249* (17), 1902−1916.

(5) Kaim, W.; Sarkar, B. Mixed Valency in Ruthenium Complexes—Coordinative Aspects. *Coord. Chem. Rev.* **2007**, *251* (3), 584−594.

(6) Endicott, J. F.; Chen, Y.-J. Electronic Coupling between Metal Ions in Cyanide-Bridged Ground State and Excited State Mixed Valence Complexes. *Coord. Chem. Rev.* **2013**, *257* (9), 1676−1698.

(7) Costuas, K.; Rigaut, S. Polynuclear Carbon-Rich Organometallic Complexes: Clarification of the Role of the Bridging Ligand in the Redox Properties. *Dalton Trans.* **2011**, *40* (21), 5643−5658.

(8) Halet, J.-F.; Lapinte, C. Charge Delocalization vs Localization in Carbon-Rich Iron Mixed-Valence Complexes: A Subtle Interplay between the Carbon Spacer and the (dppe)Cp*Fe Organometallic Electrophore. *Coord. Chem. Rev.* **2013**, *257* (9), 1584−1613.

(9) Low, P. J. Twists and Turns: Studies of the Complexes and Properties of Bimetallic Complexes Featuring Phenylene Ethynylene and Related Bridging Ligands. *Coord. Chem. Rev.* **2013**, *257* (9), 1507−1532.

(10) Tanaka, Y.; Akita, M. Organometallic Radicals of Iron and Ruthenium: Similarities and Dissimilarities of Radical Reactivity and Charge Delocalization. *Coord. Chem. Rev.* **2019**, *388*, 334−342.

(11) Gendron, F.; Groizard, T.; Le Guennic, B.; Halet, J.-F. Electronic Properties of Poly-Yne Carbon Chains and Derivatives with Transition Metal End-Groups. *Eur. J. Inorg. Chem.* **2020** *2020* (8), 667−681.

(12) Launay, J.-P. Electron Transfer in Molecular Binuclear Complexes and Relation with Electron Transport through Nano-junctions. *Coord. Chem. Rev.* **2013**, *257* (9), 1544−1554.

(13) Kim; Beebe, J. M.; Olivier, C.; Rigaut, S.; Touchard, D.; Kushmerick, J. G.; Zhu, X.-Y.; Frisbie, C. D. Temperature and Length Dependence of Charge Transport in Redox-Active Molecular Wires Incorporating Ruthenium(II) Bis(σ-Arylacetylide) Complexes. *J. Phys. Chem. C* **2007**, *111* (20), 7521−7526.

(14) Olivier, C.; Kim, B.; Touchard, D.; Rigaut, S. Redox-Active Molecular Wires Incorporating Ruthenium(II) σ-Arylacetylide Complexes for Molecular Electronics. *Organometallics* **2008**, *27* (4), 509−518.

(15) Luo, L.; Benameur, A.; Brignou, P.; Choi, S. H.; Rigaut, S.; Frisbie, C. D. Length and Temperature Dependent Conduction of Ruthenium-Containing Redox-Active Molecular Wires. *J. Phys. Chem. C* **2011**, *115* (40), 19955−19961.

(16) Schwarz, F.; Kastlunger, G.; Lissel, F.; Riel, H.; Venkatesan, K.; Berke, H.; Stadler, R.; Lörtscher, E. High-Conductive Organometallic Molecular Wires with Delocalized Electron Systems Strongly Coupled to Metal Electrodes. *Nano Lett.* **2014**, *14* (10), 5932−5940.

(17) Lissel, F.; Schwarz, F.; Blacque, O.; Riel, H.; Lörtscher, E.; Venkatesan, K.; Berke, H. Organometallic Single-Molecule Electronics: Tuning Electron Transport through X-$(Diphosphine)_2FeC_4Fe(Diphosphine)2X$ Building Blocks by Varying the Fe−X−Au Anchoring Scheme from Coordinative to Covalent. *J. Am. Chem. Soc.* **2014**, *136* (41), 14560−14569.

(18) Wuttke, E.; Hervault, Y.-M.; Polit, W.; Linseis, M.; Erler, P.; Rigaut, S.; Winter, R. F. Divinylphenylene- and Ethynylvinylphenylene-Bridged Mono-, Di-, and Triruthenium Complexes for Covalent Binding to Gold Electrodes. *Organometallics* **2014**, *33* (18), 4672−4686.

(19) Schwarz, F.; Kastlunger, G.; Lissel, F.; Egler-Lucas, C.; Semenov, S. N.; Venkatesan, K.; Berke, H.; Stadler, R.; Lörtscher, E. Field-Induced Conductance Switching by Charge-State Alternation in Organometallic Single-Molecule Junctions. *Nat. Nanotechnol.* **2016**, *11* (2), 170−176.

(20) Sugimoto, K.; Tanaka, Y.; Fujii, S.; Tada, T.; Kiguchi, M.; Akita, M. Organometallic Molecular Wires as Versatile Modules for Energy-Level Alignment of the Metal−Molecule−Metal Junction. *Chem. Commun.* **2016**, *52* (34), 5796−5799.

(21) Bu, D.; Xiong, Y.; Tan, Y. N.; Meng, M.; Low, P. J.; Kuang, D.-B.; Liu, C. Y. Understanding the Charge Transport Properties of Redox Active Metal−Organic Conjugated Wires. *Chem. Sci.* **2018**, *9* (14), 3438−3450.

(22) Tanaka, Y.; Kato, Y.; Tada, T.; Fujii, S.; Kiguchi, M.; Akita, M. Doping" of Polyyne with an Organometallic Fragment Leads to Highly Conductive Metallapolyyne Molecular Wire. *J. Am. Chem. Soc.* **2018**, *140* (32), 10080−10084.

(23) Yashiro, A.; Tanaka, Y.; Tada, T.; Fujii, S.; Nishino, T.; Akita, M. Organometallic Molecular Wires with Thioacetylene Backbones, *trans*-{RS-(C≡C)$_n$}$_2$Ru(Phosphine)$_4$: High Conductance through Non-Aromatic Bridging Linkers. *Chem. - Eur. J.* **2021**, *27* (37), 9666−9673.
(24) Ogawa, S.; Chattopadhyay, S.; Tanaka, Y.; Ohto, T.; Tada, T.; Tada, H.; Fujii, S.; Nishino, T.; Akita, M. Control of Dominant Conduction Orbitals by Peripheral Substituents in Paddle-Wheel Diruthenium Alkynyl Molecular Junctions. *Chem. Sci.* **2021**, *12* (32), 10871−10877.
(25) Tanaka, Y.; Kato, Y.; Sugimoto, K.; Kawano, R.; Tada, T.; Fujii, S.; Kiguchi, M.; Akita, M. Single-Molecule Junctions of Multinuclear Organometallic Wires: Long-Range Carrier Transport Brought about by Metal−Metal Interaction. *Chem. Sci.* **2021**, *12* (12), 4338−4344.
(26) Park, S.; Jang, J.; Tanaka, Y.; Yoon, H. J. High Seebeck Coefficient Achieved by Multinuclear Organometallic Molecular Junctions. *Nano Lett.* **2022**, *22* (23), 9693−9699.
(27) Akita, M.; Tanaka, Y. Carbon-Rich Organometallics: Application to Molecular Electronics. *Coord. Chem. Rev.* **2022**, *461*, No. 214501.
(28) Tanaka, Y.; Bae, Y.; Ogasawara, F.; Suzuki, K.; Kobayashi, S.; Kaneko, S.; Fujii, S.; Nishino, T.; Akita, M. Molecule-Electrode Interfaces Controlled by Bulky Long-Legged Ligands in Organometallic Molecular Wires. *Adv. Mater. Interfaces* **2023**, *10* (11), 2202464.
(29) Tanaka, Y. Metal Complex Molecular Junctions as Thermoelectric Devices. *Chem. - Eur. J.* **2023**, *29* (29), No. e202300472.
(30) Tanaka, Y. Organometallics in Molecular Junctions: Conductance, Functions, and Reactions. *Dalton Trans.* **2024**. *5*38512.
(31) Akita, M.; Tanaka, Y.; Naitoh, C.; Ozawa, T.; Hayashi, N.; Takeshita, M.; Inagaki, A.; Chung, M.-C. Synthesis of a Series of Diiron Complexes Based on a Tetraethynylethene Skeleton and Related C$_6$-Enediyne Spacers, (dppe)Cp*Fe-C≡CC(R)═C(R)C≡C-FeCp*(dppe): Tunable Molecular Wires. *Organometallics* **2006**, *25* (22), 5261−5275.
(32) Matsuura, Y.; Tanaka, Y.; Akita, M. *p*-Diethynylbenzene-Based Molecular Wires, ***Fe***-C≡C-*p*-C$_6$H$_2$X$_2$-C≡C-***Fe*** [***Fe*** = Fe(η^5-C$_5$Me$_5$)(dppe)]: Synthesis, Substituent Effects and Unexpected Formation of Benzodifuran Complex. *J. Organomet. Chem.* **2009**, *694* (12), 1840−1847.
(33) Speck, J. M.; Korb, M.; Rüffer, T.; Hildebrandt, A.; Lang, H. Substituent Influence on Charge Transfer Interactions in α,α'-Diferrocenylthiophenes. *Organometallics* **2014**, *33* (18), 4813−4823.
(34) Fan, Y.; Li, H.-M.; Zou, G.-D.; Zhang, X.; Pan, Y.-L.; Cao, K.-K.; Zhang, M.-L.; Ma, P.-L.; Lu, H.-T. Diferrocenes Bridged by a Geminal Diethynylethene Scaffold with Varying Pendant Substituents: Electronic Interactions in Cross-Conjugated System. *Organometallics* **2017**, *36* (21), 4278−4286.
(35) Harrison, D. P.; Grotjahn, R.; Naher, M.; Ghazvini, S. M. B. H.; Mazzucato, D. M.; Korb, M.; Moggach, S. A.; Lambert, C.; Kaupp, M.; Low, P. J. Quantum Interference in Mixed-Valence Complexes: Tuning Electronic Coupling Through Substituent Effects. *Angew. Chem., Int. Ed.* **2022**, *61* (45), No. e202211000.
(36) de Montigny, F.; Argouarch, G.; Costuas, K.; Halet, J.-F.; Roisnel, T.; Toupet, L.; Lapinte, C. Electron Transfer and Electron Exchange between [Cp*(dppe)Fe]$^{n+}$ (n = 0, 1) Building Blocks Mediated by the 9,10-Bis(Ethynyl)Anthracene Bridge. *Organometallics* **2005**, *24* (19), 4558−4572.
(37) Tanaka, Y.; Shaw-Taberlet, J. A.; Justaud, F.; Cador, O.; Roisnel, T.; Akita, M.; Hamon, J.-R.; Lapinte, C. Electronic and Magnetic Couplings in Free and π-Coordinated 1,4-Diethynylnaphthalene-Bridged [Cp*(dppe)Fe]$^{(n+)}$ (n = 0, 1) Units. *Organometallics* **2009**, *28* (16), 4656−4669.
(38) Fox, M. A.; Le Guennic, B.; Roberts, R. L.; Brue, D. A.; Yufit, D. S.; Howard, J. A. K.; Manca, G.; Halet, J.-F.; Hartl, F.; Low, P. J. Simultaneous Bridge-Localized and Mixed-Valence Character in Diruthenium Radical Cations Featuring Diethynylaromatic Bridging Ligands. *J. Am. Chem. Soc.* **2011**, *133* (45), 18433−18446.
(39) Tanaka, Y.; Koike, T.; Akita, M. 2-Dimensional Molecular Wiring Based on Toroidal Delocalization of Hexaarylbenzene. *Chem. Commun.* **2010**, *46* (25), 4529−4531.
(40) Sugimoto, K.; Idei, H.; Tanaka, Y.; Akita, M. Synthesis and Charge Delocalization Property of Multimetallic Molecular Wires with Diethynylthiophene Bridges. *J. Organomet, Chem.* **2017**, *847*, 121−131.
(41) Tanaka, Y.; Kawano, R.; Akita, M. Acene Size-Dependent Transition of The Radical Centers From the Metal to The Acene Parts In Monocationic Dinuclear (Diethynylacene)Diyl Complexes. *Chem. - Eur. J.* **2022**, *28* (55), No. e202201358.
(42) Tanaka, Y.; Koike, T.; Akita, M. Reversible, Fine Performance Tuning of an Organometallic Molecular Wire by Addition, Ligand Replacement and Removal of Dicobalt Fragments. *Eur. J. Inorg. Chem.* **2010**, *23*, 3571−3575.
(43) Tanaka, Y.; Inagaki, A.; Akita, M. A Photoswitchable Molecular Wire with the Dithienylethene (DTE) Linker, (dppe)(η^5-C$_5$Me$_5$)Fe-C≡C-DTE-C≡C-Fe(η^5-C$_5$Me$_5$)(dppe). *Chem. Commun.* **2007**, *11*, 1169−1171.
(44) Motoyama, K.; Koike, T.; Akita, M. Remarkable Switching Behavior of Bimodally Stimuli-Responsive Photochromic Dithienylethenes with Redox-Active Organometallic Attachments. *Chem. Commun.* **2008**, *44*, 5812−5814.
(45) Liu, Y.; Lagrost, C.; Costuas, K.; Tchouar, N.; Bozec, H. L.; Rigaut, S. A Multifunctional Organometallic Switch with Carbon-Rich Ruthenium and Diarylethene Units. *Chem. Commun.* **2008**, *46*, 6117−6119.
(46) Tanaka, Y.; Ishisaka, T.; Inagaki, A.; Koike, T.; Lapinte, C.; Akita, M. Photochromic Organometallics with a Dithienylethene (DTE) Bridge, [Y-C≡C-DTE-C≡C-Y] (Y = {MCp*(dppe)}): Photoswitchable Molecular Wire (M = Fe) versus Dual Photo- and Ellectrochromism (M = Ru). *Chem. - Eur. J.* **2010**, *16* (16), 4762−4776.
(47) Oyama, Y.; Kawano, R.; Tanaka, Y.; Akita, M. Dinuclear Ruthenium Acetylide Complexes with Diethynylated Anthrahydroquinone and Anthraquinone Frameworks: A Multi-Stimuli-Responsive Organometallic Switch. *Dalton Trans.* **2019**, *48* (21), 7432−7441.
(48) Launay, J.-P. Long-Distance Intervalence Electron Transfer. *Chem. Soc. Rev.* **2001**, *30* (6), 386−397.
(49) Sakurai, A.; Akita, M.; Moro-oka, Y. Synthesis and Characterization of the Dodecahexaynediyldiiron Complex, Fp*−(C≡C)$_6$−Fp* [Fp*= Fe(η^5-C$_5$Me$_5$)(CO)$_2$], the Longest Structurally Characterized Polyynediyl Complex. *Organometallics* **1999**, *18* (16), 3241−3244.
(50) Dembinski, R.; Bartik, T.; Bartik, B.; Jaeger, M.; Gladysz, J. A. Toward Metal-Capped One-Dimensional Carbon Allotropes: Wire-like C$_6$−C$_{20}$ Polyynediyl Chains That Span Two Redox-Active (η^5-C$_5$Me$_5$)Re(NO)(PPh$_3$) Endgroups. *J. Am. Chem. Soc.* **2000**, *122* (5), 810−822.
(51) Venkatesan, K.; Blacque, O.; Berke, H. Organometallic Manganese Complexes as Scaffolds for Potential Molecular Wires. *Dalton Trans.* **2007**, *11*, 1091−1100.
(52) Semenov, S. N.; Taghipourian, S. F.; Blacque, O.; Fox, T.; Venkatesan, K.; Berke, H. An Iron-Capped Metal−Organic Polyyne: {[Fe](C≡C)$_2$[W]≡CC≡CC≡[W](C≡C)$_2$[Fe]}. *J. Am. Chem. Soc.* **2010**, *132* (22), 7584−7585.
(53) Wuttke, E.; Pevny, F.; Hervault, Y.-M.; Norel, L.; Drescher, M.; Winter, R. F.; Rigaut, S. Fully Delocalized (Ethynyl)(Vinyl)Phenylene Bridged Triruthenium Complexes in up to Five Different Oxidation States. *Inorg. Chem.* **2012**, *51* (3), 1902−1915.
(54) Lissel, F.; Fox, T.; Blacque, O.; Polit, W.; Winter, R. F.; Venkatesan, K.; Berke, H. Stepwise Construction of an Iron-Substituted Rigid-Rod Molecular Wire: Targeting a Tetraferra−Tetracosa−Decayne. *J. Am. Chem. Soc.* **2013**, *135* (10), 4051−4060.
(55) Cao, Z.; Xi, B.; Jodoin, D. S.; Zhang, L.; Cummings, S. P.; Gao, Y.; Tyler, S. F.; Fanwick, P. E.; Crutchley, R. J.; Ren, T. Diruthenium−Polyyn-Diyl−Diruthenium Wires: Electronic Coupling in the Long Distance Regime. *J. Am. Chem. Soc.* **2014**, *136* (34), 12174−12183.

https://doi.org/10.1021/acsorginorgau.4c00021
ACS Org. Inorg. Au 2024, 4, 504−516

(56) Bruce, M. I.; Cole, M. L.; Ellis, B. G.; Gaudio, M.; Nicholson, B. K.; Parker, C. R.; Skelton, B. W.; White, A. H. The Series of Carbon-Chain Complexes $\{Ru(dppe)Cp*\}_2\{\mu\text{-}(C{\equiv}C)_x\}$ (x = 4−8, 11): Synthesis, Structures, Properties and Some Reactions. *Polyhedron* **2015**, *86*, 43−56.
(57) Burgun, A.; Gendron, F.; Schauer, P. A.; Skelton, B. W.; Low, P. J.; Costuas, K.; Halet, J.-F.; Bruce, M. I.; Lapinte, C. Straightforward Access to Tetrametallic Complexes with a Square Array by Oxidative Dimerization of Organometallic Wires. *Organometallics* **2013**, *32* (18), 5015−5025.
(58) Tanaka, Y.; Yashiro, A.; Akita, M. Thermally Stable Monoruthenium Acetylide Radical Species. *Synlett* **2024**, 1306 DOI: 10.1055/s-0042-1751538.
(59) Coat, F.; Lapinte, C. Molecular Wire Consisting of a C_8 Chain of Elemental Carbon Bridging Two Metal Centers: Synthesis and Characterization of $[\{Fe(\eta^5\text{-}C_5Me_5)(dppe)\}_2(\mu\text{-}C_8)]$. *Organometallics* **1996**, *15* (2), 477−479.
(60) Le Narvor, N.; Lapinte, C. 1,4-Diethynylbenzene Bridged Fe(Cp*)(dppe) Units: Mixed-Valence 35-Electron and Bisiron(III) 34-Electron Complexes. *Organometallics* **1995**, *14* (2), 634−639.
(61) Ghazala, S. I.; Paul, F.; Toupet, L.; Roisnel, T.; Hapiot, P.; Lapinte, C. Di-Organoiron Mixed Valent Complexes Featuring "$(\mu_2$-dppe$)(\eta^5\text{-}C_5Me_5)$Fe" Endgroups: Smooth Class-III to Class-II Transition Induced by Successive Insertion of 1,4-Phenylene Units in a Butadiyne-Diyl Bridge. *J. Am. Chem. Soc.* **2006**, *128* (7), 2463−2476.
(62) Karafiloglou, P.; Launay, J.-P. Comparing Electron (de)-Localization in the through Benzene and Anthracene Charge Transfer. *Chem. Phys.* **2003**, *289* (2), 231−242.
(63) Sedghi, G.; García-Suárez, V. M.; Esdaile, L. J.; Anderson, H. L.; Lambert, C. J.; Martín, S.; Bethell, D.; Higgins, S. J.; Elliott, M.; Bennett, N.; Macdonald, J. E.; Nichols, R. J. Long-Range Electron Tunnelling in Oligo-Porphyrin Molecular Wires. *Nat. Nanotechnol.* **2011**, *6* (8), 517−523.
(64) Yao, D.; Zhang, X.; Triadon, A.; Richy, N.; Mongin, O.; Blanchard-Desce, M.; Paul, F.; Paul-Roth, C. O. New Conjugated Meso-Tetrafluorenylporphyrin-Cored Derivatives as Fluorescent Two-Photon Photosensitizers for Singlet Oxygen Generation. *Chem. - Eur. J.* **2017**, *23* (11), 2635−2647.
(65) Leary, E.; Limburg, B.; Alanazy, A.; Sangtarash, S.; Grace, I.; Swada, K.; Esdaile, L. J.; Noori, M.; González, M. T.; Rubio-Bollinger, G.; Sadeghi, H.; Hodgson, A.; Agraït, N.; Higgins, S. J.; Lambert, C. J.; Anderson, H. L.; Nichols, R. J. Bias-Driven Conductance Increase with Length in Porphyrin Tapes. *J. Am. Chem. Soc.* **2018**, *140* (40), 12877−12883.
(66) Zhang, X.; Abid, S.; Shi, L.; Williams, J. A. G.; Fox, M. A.; Miomandre, F.; Tourbillon, C.; Audibert, J.-F.; Mongin, O.; Paul, F.; Paul-Roth, C. O. Fluorenylporphyrins Functionalized by Electrochromic Ruthenium Units as Redox-Triggered Fluorescence Switches. *Dalton Trans.* **2019**, *48* (31), 11897−11911.
(67) Shi, L.; Sun, Z.; Richy, N.; Blanchard-Desce, M.; Mongin, O.; Paul, F.; Paul-Roth, C. O. Giant Star-Shaped Meso-Substituted Fluorescent Porphyrins with Fluorenyl-Containing Arms Designed for Two-Photon Oxygen Photosensitization. *Chem.—Eur. J.* **2024**, *30* (13), No. e202303243.
(68) Deng, J.-R.; González, M. T.; Zhu, H.; Anderson, H. L.; Leary, E. Ballistic Conductance through Porphyrin Nanoribbons. *J. Am. Chem. Soc.* **2024**, *146* (6), 3651−3659.
(69) While MV systems combined with the metalloporphyrin-linkers have been seldom studied except for the ferrocene-based systems. See refs 70−73.
(70) Nemykin, V. N.; Barrett, C. D.; Hadt, R. G.; Subbotin, R. I.; Maximov, A. Y.; Polshin, E. V.; Koposov, A. Y. Mixed-Valence States Formation in Conformationally Flexible Metal-Free 5,10,15,20-Tetraferrocenylporphyrin and 5,10-Bisferrocenyl-15,20-Bisphenylporphyrin. *Dalton Trans.* **2007**, *31*, 3378−3389.
(71) Nemykin, V. N.; Rohde, G. T.; Barrett, C. D.; Hadt, R. G.; Sabin, J. R.; Reina, G.; Galloni, P.; Floris, B. Long-Range Electronic Communication in Free-Base Meso-Poly(Ferrocenyl)-Containing Porphyrins. *Inorg. Chem.* **2010**, *49* (16), 7497−7509.
(72) Erickson, N. R.; Holstrom, C. D.; Rhoda, H. M.; Rohde, G. T.; Zatsikha, Y. V.; Galloni, P.; Nemykin, V. N. Tuning Electron-Transfer Properties in 5,10,15,20-Tetra(1′-Hexanoylferrocenyl)Porphyrins as Prospective Systems for Quantum Cellular Automata and Platforms for Four-Bit Information Storage. *Inorg. Chem.* **2017**, *56* (8), 4716−4727.
(73) Vecchi, A.; Sabin, J. R.; Sabuzi, F.; Conte, V.; Cicero, D. O.; Floris, B.; Galloni, P.; Nemykin, V. N. Similar, Yet Different: Long-Range Metal−Metal Coupling and Electron-Transfer Processes in Metal-Free 5,10,15,20-Tetra(Ruthenocenyl)Porphyrin. *Inorg. Chem.* **2021**, *60* (11), 8227−8241.
(74) We reported metal acetylide MV complexes with metalloporphyrin linkers but a metal-dependent study has not been studied. See refs 75−77.
(75) Tanaka, Y.; Ono, M.; Akita, M. Synthesis and Wire-like Performance of Diruthenium Molecular Wire with a C≡C-Porphyrin-C≡C Linker. *J. Porphyrin Phthalocyanine* **2015**, *19* (1−3), 442−450.
(76) Mishiba, K.; Ono, M.; Tanaka, Y.; Akita, M. A Fully Charge-Delocalized Two-Dimensional Porphyrin System with Two Different ClassIII States. *Chem. - Eur. J.* **2016**, *23* (9), 2067−2076.
(77) Tanaka, Y.; Ono, M.; Akita, M. An Organometallic Molecular Wire Bearing a Manganese Porphyrin Linker: Coordination-Driven Modulation of the Metal-Metal Interaction. *Chem. Lett.* **2018**, *47* (10), 1296−1299.
(78) Schindler, J.; Kupfer, S.; Ryan, A. A.; Flanagan, K. J.; Senge, M. O.; Dietzek, B. Sterically Induced Distortions of Nickel(II) Porphyrins − Comprehensive Investigation by DFT Calculations and Resonance Raman Spectroscopy. *Coord. Chem. Rev.* **2018**, *360*, 1−16.
(79) Cheng, K.-L.; Li, H.-W.; Ng, D. K. P. Synthesis and Characterization of *Meso*-Ferrocenylethynyl 5,15-Diphenylporphyrins. *J. Organomet. Chem.* **2004**, *689* (9), 1593−1598.
(80) Paul, F.; Ellis, B. G.; Bruce, M. I.; Toupet, L.; Roisnel, T.; Costuas, K.; Halet, J.-F.; Lapinte, C. Bonding and Substituent Effects in Electron-Rich Mononuclear Ruthenium σ-Arylacetylides of the Formula $[(\mu_2\text{-dppe})(\eta^5\text{-}C_5Me_5)Ru(C{\equiv}C)\text{-}1,4\text{-}(C_6H_4)X][PF_6]_n$ (n = 0, 1; X = NO_2, CN, F, H, OMe, NH_2). *Organometallics* **2006**, *25* (3), 649−665.
(81) Murai, M.; Sugimoto, M.; Akita, M. Zinc-Porphyrins Functionalized with Redox-Active Metal Peripherals: Enhancement of dπ−pπ Interaction Leading to Unique Assembly and Redox-Triggered Remote Switching of Fluorescence. *Dalton Trans.* **2013**, *42* (45), 16108−16120.
(82) Lapinte, C. Magnetic Perturbation of the Redox Potentials of Localized and Delocalized Mixed-Valence Complexes. *J. Organomet. Chem.* **2008**, *693* (5), 793−801.
(83) Gückel, S.; Safari, P.; Bagher Hosseini Ghazvini, S. M.; Hall, M. R.; Gluyas, J. B. G.; Kaupp, M.; Low, P. J. Iron Versus Ruthenium: Evidence for the Distinct Differences in the Electronic Structures of Hexa-1,3,5-Triyn-1,6-Diyl-Bridged Complexes $[Cp*(dppe)M\}\{\mu\text{-}(C{\equiv}C)_3\}\{M(dppe)Cp*\}]^+$ (M = Fe, Ru). *Organometallics* **2021**, *40* (3), 346−357.
(84) Brunschwig, B. S.; Creutz, C.; Sutin, N. Optical Transitions of Symmetrical Mixed-Valence Systems in the Class II−III Transition Regime. *Chem. Soc. Rev.* **2002**, *31* (3), 168−184.
(85) Relatively symmetric band shape of IVCT indicate the classification of class IV MV species. See ref 86.
(86) Tan, Y. N.; Cheng, T.; Meng, M.; Zhang, Y. Y.; Liu, C. Y.; Sun, M. F.; Zhang, Y.; Low, P. J. Optical Behaviors and Electronic Properties of Mo_2−Mo_2 Mixed-Valence Complexes within or beyond the Class III Regime: Testing the Limits of the Two-State Model. *J. Phys. Chem. C* **2017**, *121* (50), 27860−27873.
(87) Paul, F.; Toupet, L.; Thépot, J.-Y.; Costuas, K.; Halet, J.-F.; Lapinte, C. Electron-Rich Piano-Stool Iron σ-Acetylides. Electronic Structures of Arylalkynyl Iron(III) Radical Cations. *Organometallics* **2005**, *24* (22), 5464−5478.

https://doi.org/10.1021/acsorginorgau.4c00021
ACS Org. Inorg. Au 2024, 4, 504−516

(88) Makhoul, R.; Sahnoune, H.; Dorcet, V.; Halet, J.-F.; Hamon, J.-R.; Lapinte, C. 1,2-Diethynylbenzene-Bridged [Cp*(dppe)Fe]$^{n+}$ Units: Effect of Steric Hindrance on the Chemical and Physical Properties. *Organometallics* **2015**, *34* (13), 3314−3326.
(89) Roué, S.; Sahnoune, H.; Toupet, L.; Halet, J.-F.; Lapinte, C. Double Insertion of Thiophene Rings in Polyynediyl Chains to Stabilize Nanoscaled Molecular Wires with [Cp*(dppe)Fe] Termini. *Organometallics* **2016**, *35* (12), 2057−2070.
(90) Kojima, T.; Nakanishi, T.; Honda, T.; Harada, R.; Shiro, M.; Fukuzumi, S. Impact of Distortion of Porphyrins on Axial Coordination in (Porphyrinato)Zinc(II) Complexes with Aminopyridines as Axial Ligands. *Eur. J. Inorg. Chem.* **2009**, *2009* (6), 727−734.
(91) Formation of the 1:1 adduct of [$\mathbf{1}^{\mathbf{FeZn}}$]$^{+\bullet}$ with pyridine was confirmed by elemental analysis and ESI-MS spectrum.
(92) Lambert, C.; Nöll, G.; Schelter, J. Bridge-Mediated Hopping or Superexchange Electron-Transfer Processes in Bis(Triarylamine) Systems. *Nat. Mater.* **2002**, *1* (1), 69−73.
(93) DFT calculations of $\mathbf{1}^{\mathbf{"FeZn}}$ and ($\mathbf{1}^{\mathbf{"FeZn}}$)•DMAP were performed at the B3LYP/LanL2DZ,6-31G(d) level. In the optimized structure of ($\mathbf{1}^{\mathbf{"FeZn}}$)•DMAP, the porphyrin moiety did not show the distorted structure.
(94) Pangborn, A. B.; Giardello, M. A.; Grubbs, R. H.; Rosen, R. K.; Timmers, F. J. Safe and Convenient Procedure for Solvent Purification. *Organometallics* **1996**, *15* (5), 1518−1520.
(95) Taylor, P. N.; Anderson, H. L. Cooperative Self-Assembly of Double-Strand Conjugated Porphyrin Ladders. *J. Am. Chem. Soc.* **1999**, *121* (49), 11538−11545.
(96) Plater, M. J.; Aiken, S.; Bourhill, G. A New Synthetic Route to Donor−Acceptor Porphyrins. *Tetrahedron* **2002**, *58* (12), 2405−2413.
(97) Monnereau, C.; Blart, E.; Montembault, V.; Fontaine, L.; Odobel, F. Synthesis of New Crosslinkable Co-Polymers Containing a Push−Pull Zinc Porphyrin for Non-Linear Optical Applications. *Tetrahedron* **2005**, *61* (42), 10113−10121.
(98) Oda, K.; Akita, M.; Hiroto, S.; Shinokubo, H. Silylethynyl Substituents as Porphyrin Protecting Groups for Solubilization and Selectivity Control. *Org. Lett.* **2014**, *16* (6), 1818−1821.
(99) Mays, M. J.; Sears, P. L. Preparation and Mössbauer Spectra of Some Cyclopentadienyl Iron Complexes Containing a Chelating Diphosphine Ligand. *J. Chem. Soc., Dalton Trans.* **1973**, *18*, 1873−1875.
(100) Roger, C.; Hamon, P.; Toupet, L.; Rabaa, H.; Saillard, J. Y.; Hamon, J. R.; Lapinte, C. Halo- and Alkyl-(Pentamethylcyclopentadienyl)[1,2-Bis(Diphenylphosphino)Ethane]-Iron(III) 17-Electron Complexes: Synthesis, NMR and Magnetic Properties and EHMO Calculations. *Organometallics* **1991**, *10* (4), 1045−1054.
(101) Oshima, N.; Suzuki, H.; Moro-Oka, Y. Synthesis and Some Reactions of Dichloro(pentamethylcyclopentadienyl)Ruthenium(Iii) Oligomer. *Chem. Lett.* **1984**, *13* (7), 1161−1164.
(102) Bruce, M. I.; Ellis, B. G.; Low, P. J.; Skelton, B. W.; White, A. H. Syntheses, Structures, and Spectro-Electrochemistry of {Cp*(PP)-Ru}C≡CC≡C{Ru(PP)Cp*} (PP = dppm, dppe) and Their Mono- and Dications. *Organometallics* **2003**, *22* (16), 3184−3198.
(103) Frisch, M. J.; Trucks, G. W.; Schlegel, H. B.; Scuseria, G. E.; Robb, M. A.; Cheeseman, J. R.; Scalmani, G.; Barone, V.; Petersson, G. A.; Nakatsuji, H.; Li, X.; Caricato, M.; Marenich, A. V.; Bloino, J.; Janesko, B. G.; Gomperts, R.; Mennucci, B.; Hratchian, H. P.; Ortiz, J. V.; Izmaylov, A. F.; Sonnenberg, J. L.; D., Williams-Young, Ding, F.; Lipparini, F.; Egidi, F.; Goings, J.; Peng, B.; Petrone, A.; Henderson, T.; Ranasinghe, D.; Zakrzewski, V. G.; Gao, J.; Rega, N.; Zheng, G.; Liang, W.; Hada, M.; Ehara, M.; Toyota, K.; Fukuda, R.; Hasegawa, J.; Ishida, M.; Nakajima, T.; Honda, Y.; Kitao, O.; Nakai, H.; Vreven, T.; Throssell, K.; Montgomery, J. A., Jr., Peralta, J. E.; Ogliaro, F.; Bearpark, M. J.; Heyd, J. J.; Brothers, E. N.; Kudin, K. N.; Staroverov, V. N.; Keith, T. A.; Kobayashi, R.; Normand, J.; Raghavachari, K.; Rendell, A. P.; Burant, J. C.; Iyengar, S. S.; Tomasi, J.; Cossi, M.; Millam, J. M.; Klene, M.; Adamo, C.; Cammi, R.; Ochterski, J. W.; Martin, R. L.; Morokuma, K.; Farkas, O.; Foresman, J. B., Fox, D. J.; *Gaussian 16*, Revision B.01, Gaussian, Inc., Wallingford CT, 2016.
(104) Parthey, M.; Kaupp, M. Quantum-Chemical Insights into Mixed-Valence Systems: Within and beyond the Robin−Day Scheme. *Chem. Soc. Rev.* **2014**, *43* (14), 5067−5088.

https://doi.org/10.1021/acsorginorgau.4c00021
ACS Org. Inorg. Au 2024, 4, 504−516